

PAPER • OPEN ACCESS

Frequency–frequency correlations of single-trajectory spectral densities of Gaussian processes

To cite this article: Alessio Squarcini *et al* 2022 *New J. Phys.* **24** 093031

View the [article online](#) for updates and enhancements.

You may also like

- [MASS-ANGULAR-MOMENTUM RELATIONS IMPLIED BY MODELS OF TWIN PEAK QUASI-PERIODIC OSCILLATIONS](#)
Gabriel Török, Pavel Bakala, Eva Šrámková *et al.*
- [Effects of degree-frequency correlations on network synchronization: Universality and full phase-locking](#)
P. S. Skardal, J. Sun, D. Taylor *et al.*
- [CORRELATIONS IN THE \(SUB\)MILLIMETER BACKGROUND FROM ACT x BLAST](#)
Amir Hajian, Marco P. Viero, Graeme Addison *et al.*



PAPER

Frequency–frequency correlations of single-trajectory spectral densities of Gaussian processes

OPEN ACCESS

RECEIVED
31 May 2022REVISED
23 August 2022ACCEPTED FOR PUBLICATION
5 September 2022PUBLISHED
27 September 2022Original content from
this work may be used
under the terms of the
[Creative Commons
Attribution 4.0 licence](#).Any further distribution
of this work must
maintain attribution to
the author(s) and the
title of the work, journal
citation and DOI.Alessio Squarcini^{1,2,3,*} , Enzo Marinari^{4,5} , Gleb Oshanin⁶ , Luca Peliti⁷
and Lamberto Rondoni^{8,9} ¹ Institut für Theoretische Physik, Universität Innsbruck, Technikerstrasse 21A, A-6020 Innsbruck, Austria² Max-Planck-Institut für Intelligente Systeme, Heisenbergstr. 3, D-70569, Stuttgart, Germany³ IV. Institut für Theoretische Physik, Universität Stuttgart, Pfaffenwaldring 57, D-70569 Stuttgart, Germany⁴ Dipartimento di Fisica, Sapienza Università di Roma, P.le A. Moro 2, I-00185 Roma, Italy⁵ INFN, Sezione di Roma 1 and Nanotech-CNR, UOS di Roma, P.le A. Moro 2, I-00185 Roma, Italy⁶ Sorbonne Université, CNRS, Laboratoire de Physique Théorique de la Matière Condensée (UMR CNRS 7600), 4 place Jussieu, 75252 Paris Cedex 05, France⁷ Santa Marinella Research Institute, Santa Marinella, Italy⁸ Dipartimento di Scienze Matematiche, Politecnico di Torino, Corso Duca degli Abruzzi 24, 10129 Torino, Italy⁹ INFN, Sezione di Torino, Via P. Giuria 1, 10125 Torino, Italy

* Author to whom any correspondence should be addressed.

E-mail: alessio.squarcini@uibk.ac.at**Keywords:** Gaussian stochastic process, power spectral density, frequency–frequency correlation function**Abstract**

We investigate the stochastic behavior of the single-trajectory spectral density $S(\omega, \mathcal{T})$ of several Gaussian stochastic processes, i.e., Brownian motion, the Ornstein–Uhlenbeck process, the Brownian gyrator model and fractional Brownian motion, as a function of the frequency ω and the observation time \mathcal{T} . We evaluate in particular the variance and the frequency–frequency correlation of $S(\omega, \mathcal{T})$ for different values of ω . We show that these properties exhibit different behaviors for different physical cases and can therefore be used as a sensitive probe discriminating between different kinds of random motion. These results may prove quite useful in the analysis of experimental and numerical data.

1. Introduction

The power spectral density (PSD) of a stochastic process contains a wealth of information on its temporal evolution and correlations. In particular, the asymptotics of the frequency dependence of the PSD of a diffusion process characterise the short- and large-time behaviour of the process under consideration and can often discriminate anomalous from standard behavior (see, e.g., [1–11]). As a consequence, a substantial knowledge of the PSDs of rather diverse processes has nowadays been accumulated. Examples contain, for instance, the spectral analysis of time-series associated with the loudness of musical recordings [12, 13], noise in graphene devices [14], evolution of climate data [15], fluorescence intermittency in nanosystems [16], time gaps between large earthquakes [17], current fluctuations in nanoscale electrodes [18] and across nanopores [19], statistics of blinking quantum dots [20], dynamics of tracers in artificially crowded fluids [21], as well as the evolution of velocities of motile amoebae [22, 23], trajectories of nano-machines, e.g., of the Brownian gyrator (BG) [24, 25], of active Brownian motion [26], of anomalously diffusing walkers evolving in optical traps [27], and of membrane proteins and other subordinated random walks [28]. Other examples can be found, e.g., in [29].

In most of these works, the attention is focused on the limit, for the observation time \mathcal{T} going to infinity, of the average $\mu(\omega, \mathcal{T}) = \overline{S(\omega, \mathcal{T})}$ of the PSD over all realizations of the process for a given (angular) frequency ω (see, e.g., [1]). However, since $S(\omega, \mathcal{T})$ for each realization of the process is a random quantity, there is a great deal of untapped information in the statistical properties of the single-trajectory PSD. This information can be experimentally retrieved thanks to the recent progress in tracking trajectories

of individual particles. One can thus be interested, e.g., in the variance of $S(\omega, \mathcal{T})$ or in the correlation of the spectral density for two different values of ω for the same realization.

These questions have been addressed in particular for the time series associated with blinking events in quantum dots [3], in standard Brownian motion [30] and in several anomalous diffusion processes [31–34], and also for the trajectories of the BG [35]. For instance, in [3] (see also [1] for some other examples) the distribution of $S(\omega, \mathcal{T})$ was obtained for the time series of blinking events in quantum dots, and shown to converge to the exponential function in the limit $\mathcal{T} \rightarrow \infty$. However, this is the only system, to our knowledge, in which the frequency–frequency correlation of the PSD has been analyzed [3]. It is therefore interesting to investigate the behavior of the frequency–frequency correlation of the PSD in different Gaussian processes.

It was shown for several distinct examples of centered Gaussian processes,¹⁰ that the probability distribution function (PDF) of $S(\omega, \mathcal{T})$ has a universal expression that depends only on its average $\mu(\omega, \mathcal{T})$ and on its coefficient of variation $\gamma(\omega, \mathcal{T})$, defined by

$$\gamma(\omega, \mathcal{T}) = \frac{\sqrt{S^2(\omega, \mathcal{T}) - \mu^2(\omega, \mathcal{T})}}{\mu(\omega, \mathcal{T})}. \quad (1)$$

The explicit form of the PDF for these processes implies that $\gamma(\omega, \mathcal{T})$ satisfies the crucial two-sided inequality

$$1 \leq \gamma \leq \sqrt{2}. \quad (2)$$

This has the consequence in particular that fluctuations of the PSD are generically larger than its mean value. It was shown in [36] that this inequality holds in general for centered Gaussian processes.

It was also shown, for the same processes as above, that $\gamma(\omega, \mathcal{T})$ depends on the frequency and the observation time only via the product $\omega\mathcal{T}$. Importantly, for fixed $\omega > 0$ and $\mathcal{T} \rightarrow \infty$, the coefficient of variation approaches a constant ω -independent value, dependent only on the spread of the process. It was thus suggested [31] (see also [32]) that γ can also serve as a robust criterion of anomalous diffusion—the issue to which we will return at the end of this paper. Moreover, the PDF reached in the $\mathcal{T} \rightarrow \infty$ limit depends on $S(\omega) = \lim_{\mathcal{T} \rightarrow \infty} S(\omega, \mathcal{T})$ and on its average $\mu(\omega)$ only in the combination

$$b_\omega = \frac{S(\omega)}{\mu(\omega)}. \quad (3)$$

Therefore, in the limit of infinite observation time, the statistical properties of $S(\omega, \mathcal{T})$ are summarized by those of the random variables b_ω for different values of ω . It is therefore natural to investigate the properties of these variables, and in particular of their mutual dependence for different values of ω . It was shown in particular that for the blinking quantum dots [3] and also for some bounded processes (see [1]) the values of b_ω for different values of ω are totally uncorrelated. However, in processes of different kinds these quantities can in principle fit in three possible scenarios, namely (1) they could be totally correlated, i.e., the Pearson correlation coefficient $\rho(\omega_1, \omega_2)$ (see the definition in equation (10) below) of the single-trajectory spectral densities evaluated at two different frequencies will tend to 1 when $\mathcal{T} \rightarrow \infty$, or (2) be only partially correlated, such that $\rho(\omega_1, \omega_2) \rightarrow \text{const.} < 1$ in this limit, or (3) fully uncorrelated with $\rho(\omega_1, \omega_2) \rightarrow 0$.

In this paper we determine the frequency–frequency correlation function and the Pearson correlation coefficient of several Gaussian stochastic processes, i.e., the standard Brownian motion, the Ornstein–Uhlenbeck process, the out-of-equilibrium BG model and a family of anomalous diffusion processes—i.e., fractional Brownian motion (FBM) with the Hurst index $H \in (0, 1)$. We show that, depending on the process under consideration, in the limit $\mathcal{T} \rightarrow \infty$ all three above-mentioned scenarios can be realised such that, in principle, the two-frequency correlations of b_ω can serve as a robust criterion of anomalous diffusion for the analysis of experimentally-recorded trajectories or big data series, and in some aspects may be even more advantageous than γ , which was suggested for this purpose in [31, 32]. Moreover, we realise that the behavior of the correlations for finite observation time \mathcal{T} is very rich and exhibits different properties when one of the frequencies is kept equal to zero.

In section 2 we present, for an arbitrary Gaussian process, general expressions for the frequency–frequency correlation function and for the associated Pearson correlation coefficient. In section 3 we discuss in detail the cases of standard Brownian motion and standard Ornstein–Uhlenbeck process. Section 4 is devoted to the analysis of expressions of the correlations and of the Pearson coefficient for a BG model, while in section 5 we discuss the rich behaviour of the frequency–frequency correlations of

¹⁰ These examples include standard Brownian motion [30], fractional Brownian motion with Hurst index $H \in (0, 1)$ [31] and this process in presence of localisation errors [32], scaled Brownian motion [33], several kinds of diffusing-diffusivity model [34], as well as the Brownian gyrator model [35].

a single-trajectory PSD in case of the FBM with arbitrary Hurst index H . In section 6 we conclude with a brief summary of our results and a discussion. Some details of the (rather lengthy) intermediate calculations for FBM are relegated to appendix A.

2. General framework

In this section we sketch the method to evaluate the frequency–frequency correlation function of the PSD for a general Gaussian process.

The single-trajectory spectral density $S(\omega, \mathcal{T})$ of the process $X(t)$ is defined by

$$S(\omega, \mathcal{T}) = \frac{1}{\mathcal{T}} \left| \int_0^{\mathcal{T}} dt e^{i\omega t} X(t) \right|^2. \quad (4)$$

With this definition, the frequency–frequency correlation function of $S(\omega, \mathcal{T})$ is given by

$$\begin{aligned} \overline{S(\omega_1, \mathcal{T})S(\omega_2, \mathcal{T})} &= \frac{1}{\mathcal{T}^2} \int_0^{\mathcal{T}} dt_1 \int_0^{\mathcal{T}} dt_2 \int_0^{\mathcal{T}} dt_3 \int_0^{\mathcal{T}} dt_4 \overline{X(t_1)X(t_2)X(t_3)X(t_4)} \\ &\quad \times \cos(\omega_1(t_1 - t_2)) \cos(\omega_2(t_3 - t_4)). \end{aligned} \quad (5)$$

Concentrating from now on exclusively on Gaussian processes $X(t)$, we take advantage of Wick's probability theorem [37] to obtain

$$\overline{X(t_1)X(t_2)X(t_3)X(t_4)} = \overline{X(t_1)X(t_2)}\overline{X(t_3)X(t_4)} + \overline{X(t_1)X(t_3)}\overline{X(t_2)X(t_4)} + \overline{X(t_1)X(t_4)}\overline{X(t_2)X(t_3)}. \quad (6)$$

Noticing next that the second and the third terms on the right-hand-side of the latter expression provide identical contributions to $\overline{S(\omega_1, \mathcal{T})S(\omega_2, \mathcal{T})}$, we rewrite equation (5) in the form

$$\begin{aligned} \overline{S(\omega_1, \mathcal{T})S(\omega_2, \mathcal{T})} &= \frac{1}{\mathcal{T}^2} \int_0^{\mathcal{T}} dt_1 \int_0^{\mathcal{T}} dt_2 \overline{X(t_1)X(t_2)} \cos(\omega_1(t_1 - t_2)) \\ &\quad \times \int_0^{\mathcal{T}} dt_3 \int_0^{\mathcal{T}} dt_4 \overline{X(t_3)X(t_4)} \cos(\omega_2(t_3 - t_4)) \\ &\quad + \frac{2}{\mathcal{T}^2} \int_0^{\mathcal{T}} dt_1 \int_0^{\mathcal{T}} dt_2 \int_0^{\mathcal{T}} dt_3 \int_0^{\mathcal{T}} dt_4 \overline{X(t_1)X(t_3)} \overline{X(t_2)X(t_4)} \\ &\quad \times \cos(\omega_1(t_1 - t_2)) \cos(\omega_2(t_3 - t_4)) \\ &= \mu(\omega_1, \mathcal{T}) \mu(\omega_2, \mathcal{T}) + J(\omega_1, \omega_2), \end{aligned}$$

where

$$\mu(\omega, \mathcal{T}) = \overline{S(\omega, \mathcal{T})}, \quad (7)$$

is the mean spectral density at frequency ω , while $J(\omega_1, \omega_2)$ is given by

$$\begin{aligned} J(\omega_1, \omega_2) &= \frac{2}{\mathcal{T}^2} \int_0^{\mathcal{T}} dt_1 \int_0^{\mathcal{T}} dt_2 \int_0^{\mathcal{T}} dt_3 \int_0^{\mathcal{T}} dt_4 \overline{X(t_1)X(t_3)} \overline{X(t_2)X(t_4)} \times \cos(\omega_1(t_1 - t_2)) \cos(\omega_2(t_3 - t_4)) \\ &= 2W_{cc}^2(\omega_1, \omega_2; \mathcal{T}) + 2W_{ss}^2(\omega_1, \omega_2; \mathcal{T}) + 2W_{cs}^2(\omega_1, \omega_2; \mathcal{T}) + 2W_{cs}^2(\omega_1, \omega_2; \mathcal{T}). \end{aligned} \quad (8)$$

Here we have defined

$$\begin{aligned} W_{cc}(\omega_1, \omega_2; \mathcal{T}) &= \frac{1}{\mathcal{T}} \int_0^{\mathcal{T}} dt_1 \int_0^{\mathcal{T}} dt_2 \overline{X(t_1)X(t_2)} \cos(\omega_1 t_1) \cos(\omega_2 t_2), \\ W_{ss}(\omega_1, \omega_2; \mathcal{T}) &= \frac{1}{\mathcal{T}} \int_0^{\mathcal{T}} dt_1 \int_0^{\mathcal{T}} dt_2 \overline{X(t_1)X(t_2)} \sin(\omega_1 t_1) \sin(\omega_2 t_2), \\ W_{cs}(\omega_1, \omega_2; \mathcal{T}) &= \frac{1}{\mathcal{T}} \int_0^{\mathcal{T}} dt_1 \int_0^{\mathcal{T}} dt_2 \overline{X(t_1)X(t_2)} \cos(\omega_1 t_1) \sin(\omega_2 t_2), \\ W_{cs}(\omega_1, \omega_2; \mathcal{T}) &= \frac{1}{\mathcal{T}} \int_0^{\mathcal{T}} dt_1 \int_0^{\mathcal{T}} dt_2 \overline{X(t_1)X(t_2)} \sin(\omega_1 t_1) \cos(\omega_2 t_2). \end{aligned} \quad (9)$$

We stress that the expressions (7) to (9) hold for arbitrary Gaussian processes. Correspondingly, the Pearson correlation coefficient of the random variables $S(\omega_1, \mathcal{T})$ and $S(\omega_2, \mathcal{T})$, defined by

$$\rho(\omega_1, \omega_2) = \frac{\overline{S(\omega_1, \mathcal{T})S(\omega_2, \mathcal{T})} - \mu(\omega_1, \mathcal{T})\mu(\omega_2, \mathcal{T})}{\sqrt{(\overline{S^2(\omega_1, \mathcal{T})} - \mu^2(\omega_1, \mathcal{T}))(\overline{S^2(\omega_2, \mathcal{T})} - \mu^2(\omega_2, \mathcal{T}))}}, \quad (10)$$

is given by

$$\rho(\omega_1, \omega_2) = \frac{J(\omega_1, \omega_2)}{\sqrt{J(\omega_1, \omega_1)J(\omega_2, \omega_2)}}, \quad (11)$$

an expression which also holds for an arbitrary Gaussian process.

Lastly, we note that the covariance function in the frequency domain of the random amplitude b_ω defined in (3) can be formally expressed through the Pearson correlation coefficient via the relation

$$\overline{b_{\omega_1}b_{\omega_2}} = \frac{\overline{S(\omega_1, \mathcal{T})S(\omega_2, \mathcal{T})}}{\mu(\omega_1, \mathcal{T})\mu(\omega_2, \mathcal{T})} = 1 + \gamma(\omega_1, \mathcal{T})\gamma(\omega_2, \mathcal{T})\rho(\omega_1, \omega_2), \quad (12)$$

where $\gamma(\omega, \mathcal{T})$ is the coefficient of variation defined in equation (1). As we show in what follows, $\overline{b_{\omega_1}b_{\omega_2}}$ attains distinctly different values for Gaussian sub-diffusive processes, Brownian motion and super-diffusive processes, and thus offers an interesting criterion that permits to distinguish between these three cases from the analysis of correlations of b in the frequency domain.

3. Brownian motion and the Ornstein–Uhlenbeck process

As a warming-up exercise, we start with two ‘simple’ cases, namely, the standard Brownian motion (BM) and the Ornstein–Uhlenbeck (OU) process, for which we can obtain comparatively compact expressions that hold for arbitrary frequencies and observation times.

3.1. Brownian motion

The trajectory $X(t)$ of a BM satisfies the stochastic Langevin equation

$$\dot{X} = \zeta(t), \quad (13)$$

where the dot stands for the time derivative, the viscosity is set for simplicity equal to unity, and ζ is a Gaussian zero-mean white noise satisfying

$$\overline{\zeta(t)} = 0, \quad \overline{\zeta(t)\zeta(t')} = 2k_B T \delta(t - t'), \quad (14)$$

where k_B is the Boltzmann constant (set to 1 from now on), and $\delta(t)$ is Dirac’s delta function. Equations (13) and (14) imply that the two-time correlation function $\overline{X(t_1)X(t_2)}$ obeys

$$\overline{X(t_1)X(t_2)} = 2T \min(t_1, t_2). \quad (15)$$

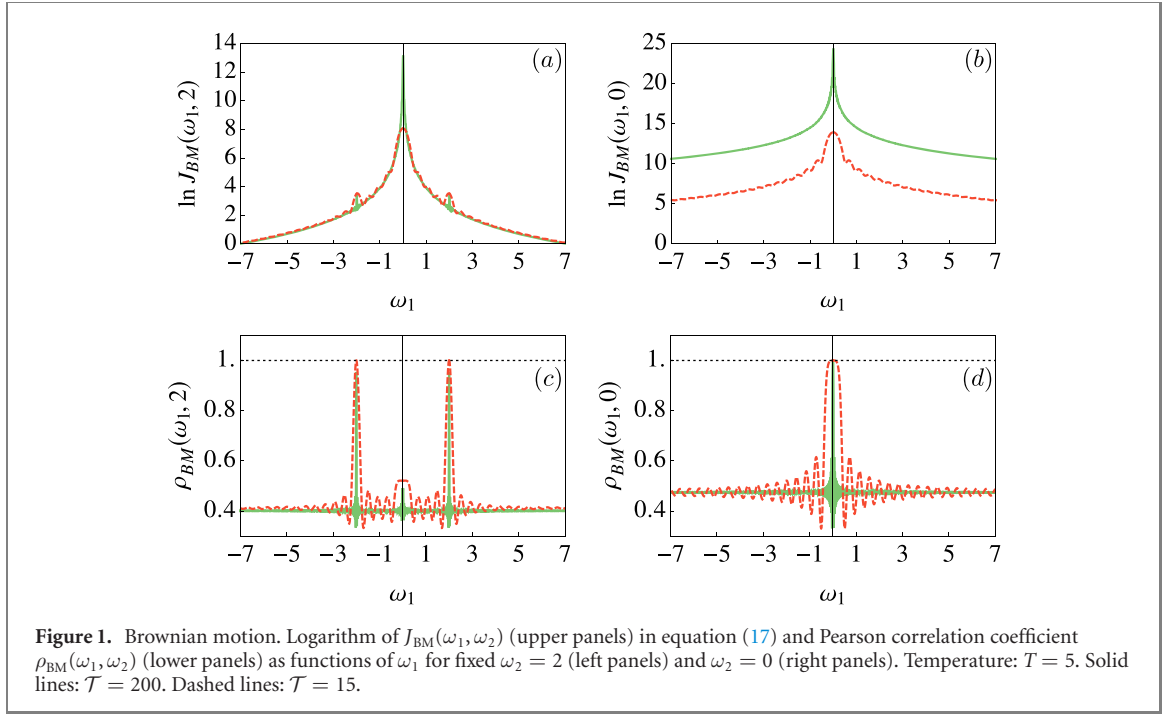
As a consequence, for the BM, the standard spectral density $\mu(\omega, \mathcal{T})$, defined in equation (7), is given for arbitrary ω and \mathcal{T} by

$$\mu(\omega, \mathcal{T}) = \frac{4T}{\omega^2} \left[1 - \frac{\sin(\omega\mathcal{T})}{\omega\mathcal{T}} \right] \quad \mu(\omega) = \lim_{\mathcal{T} \rightarrow \infty} \mu(\omega, \mathcal{T}) = \frac{4T}{\omega^2}. \quad (16)$$

See, e.g. [30] for more details.

Next, inserting the expression (15) into equation (8) and integrating, we find the following exact expression, which is valid for arbitrary frequencies and observation times:

$$\begin{aligned} J_{\text{BM}}(\omega_1, \omega_2) = & \frac{8T^2}{\omega_1^2 \omega_2^2} \left[1 - \frac{2 \sin(\omega_1 \mathcal{T})}{\omega_1 \mathcal{T}} - \frac{2 \sin(\omega_2 \mathcal{T})}{\omega_2 \mathcal{T}} \right. \\ & + \frac{2(\omega_1 \sin(\omega_1 \mathcal{T}) \cos(\omega_2 \mathcal{T}) - \omega_2 \sin(\omega_2 \mathcal{T}) \cos(\omega_1 \mathcal{T}))}{(\omega_1^2 - \omega_2^2) \mathcal{T}} \\ & + \frac{2(\omega_1^6 + \omega_2^6)}{\omega_1^2 \omega_2^2 (\omega_1^2 - \omega_2^2)^2 \mathcal{T}^2} - \frac{2(\omega_1^2 + \omega_2^2)(\omega_1^2 \cos(\omega_2 \mathcal{T}) - \omega_2^2 \cos(\omega_1 \mathcal{T}))}{\omega_1^2 \omega_2^2 (\omega_1^2 - \omega_2^2) \mathcal{T}^2} \\ & \left. - \frac{2((\omega_1^2 + \omega_2^2) \cos(\omega_1 \mathcal{T}) \cos(\omega_2 \mathcal{T}) + 2\omega_1 \omega_2 \sin(\omega_1 \mathcal{T}) \sin(\omega_2 \mathcal{T}))}{(\omega_1^2 - \omega_2^2)^2 \mathcal{T}^2} \right]. \end{aligned} \quad (17)$$



We show in figure 1 (upper panels) $J_{\text{BM}}(\omega_1, \omega_2)$ as a function of ω_1 for $\omega_2 = 2$ and $\omega_2 = 0$, and for $T = 15$ and $T = 200$. The y -axis is logarithmic since the variation range of J_{BM} is large, in particular as a function of T when one of the frequencies vanishes.

The behaviour of $J_{\text{BM}}(\omega_1, \omega_2)$ is rather rich and deserves a detailed discussion. First of all, $J_{\text{BM}}(\omega_1, \omega_2)$ is an oscillatory and symmetrical function of both frequencies. When, e.g., ω_2 is kept fixed at a nonzero value, $J_{\text{BM}}(\omega_1, \omega_2)$ exhibits pronounced peaks at $\omega_1 = 0$ and at $\omega_1 = \pm\omega_2$ (see panels (a) and (b) in figure 1). In this case, the height of the two peaks at $\omega_1 = \pm\omega_2 = \omega$ is given by

$$J_{\text{BM}}(\omega, \omega) = \frac{20T^2}{\omega^4} \left[1 + \frac{\sin(2\omega T)}{5\omega T} - \frac{12 \sin(\omega T)}{5\omega T} + \frac{17}{10\omega^2 T^2} - \frac{8 \cos(\omega T)}{5\omega^2 T^2} - \frac{\cos(2\omega T)}{10\omega^2 T^2} \right]. \quad (18)$$

This expression approaches $20T^2/\omega^4$ as $T \rightarrow \infty$. Consequently, the height of the peak at $\omega_1 = \pm\omega_2$ vanishes as ω^{-4} when $\omega \rightarrow \infty$. In turn, the height of the peak at $\omega_1 = 0$ (for $\omega_2 \neq 0$) is given by

$$J_{\text{BM}}(0, \omega_2) = \frac{2T^2 T^2}{\omega_2^2} \left[1 - \frac{4 \sin(\omega_2 T)}{\omega_2 T} + \frac{8}{\omega_2^2 T^2} - \frac{4 \cos(\omega_2 T)}{\omega_2^2 T^2} - \frac{8 \sin(\omega_2 T)}{\omega_2^3 T^3} + \frac{8}{\omega_2^4 T^4} - \frac{8 \cos(\omega_2 T)}{\omega_2^4 T^4} \right]. \quad (19)$$

Consequently, in the leading order in T , $J_{\text{BM}}(0, \omega_2)$ grows proportionally to T^2 and decreases as the frequency ω_2 grows. On the other hand, when $\omega_2 = 0$ there is a single peak at $\omega_1 = 0$ (see panel (b) in figure 1), whose height is given by

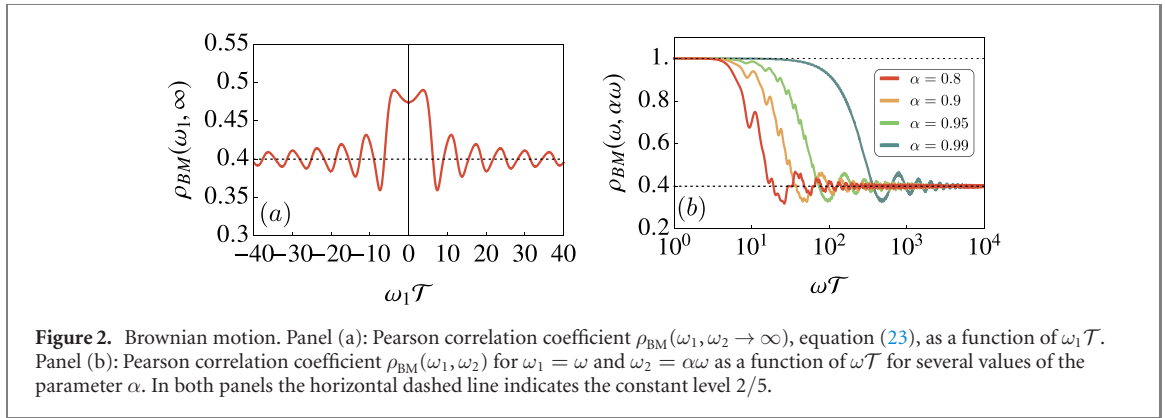
$$J_{\text{BM}}(0, 0) = \frac{8T^2}{9} T^4, \quad (20)$$

i.e., it is a monotonically increasing function of the observation time T .

We now discuss the leading large- T behaviour of the Pearson correlation coefficient $\rho_{\text{BM}}(\omega_1, \omega_2)$ (see panels (c) and (d) in figure 1). For $\omega_2 \neq 0$, we obviously have $\rho_{\text{BM}}(\omega_1, \omega_2) = 1$ at $\omega_1 = \pm\omega_2$. On the other hand, $\rho_{\text{BM}}(\omega_1, \omega_2)$ does not vanish for $\omega_1 \neq \omega_2$ when neither frequency vanishes, but approaches in the large- T limit the constant value

$$\rho_{\text{BM}}(\omega_1, \omega_2) = \frac{2}{5}. \quad (21)$$

This means that the single-trajectory PSDs $S(\omega_1, T \rightarrow \infty)$ and $S(\omega_2, T \rightarrow \infty)$ remain correlated for arbitrary different values ω_1 and ω_2 . Moreover, the Pearson coefficient exhibits an additional peak at



$\omega_1 \neq 0$, whose value approaches

$$\rho_{\text{BM}}(\omega_1 = 0, \omega_2 \neq 0) = \frac{3}{2\sqrt{10}} \approx 0.474, \tag{22}$$

in the limit $\mathcal{T} \rightarrow \infty$. Consequently, there is some excess correlation between $S(\omega, \mathcal{T} \rightarrow \infty)$ for non-vanishing ω and $S(0, \mathcal{T} \rightarrow \infty)$. We note in passing that $S(0, \mathcal{T})$ is formally given by the squared area under the random curve $X(t)$, divided by \mathcal{T} .

Further on, we consider the behaviour at finite observation time and focus on two special cases: (a) ω_1 is fixed, while $\omega_2 \rightarrow \infty$, (i.e., we quantify the correlations between $S(\omega_1, \mathcal{T})$ and $S(\infty, \mathcal{T})$), and (b) $\omega_1 = \omega$ while $\omega_2 = \alpha\omega$, where $\alpha \leq 1$ is a scale parameter. In the case (a), the Pearson correlation coefficient is given by

$$\begin{aligned} \rho_{\text{BM}}(\omega_1, \omega_2 \rightarrow \infty) &= \frac{J_{\text{BM}}(\omega_1, \infty)}{\sqrt{J_{\text{BM}}(\omega_1, \omega_1)J_{\text{BM}}(\infty, \infty)}} \\ &= \frac{2}{5} \frac{1 - \frac{2 \sin(\omega_1 \mathcal{T})}{\omega_1 \mathcal{T}} + \frac{2(1 - \cos(\omega_1 \mathcal{T}))}{\omega_1^2 \mathcal{T}^2}}{\sqrt{1 + \frac{\sin(2\omega_1 \mathcal{T}) - 12 \sin(\omega_1 \mathcal{T})}{5\omega_1 \mathcal{T}} + \frac{17 - 16 \cos(\omega_1 \mathcal{T}) - \cos(2\omega_1 \mathcal{T})}{10\omega_1^2 \mathcal{T}^2}}}, \end{aligned} \tag{23}$$

and hence is a function of the product $\omega_1 \mathcal{T}$ only. Its behavior is shown in figure 2, panel (a) as a function of the product $\omega_1 \mathcal{T}$. One can see that the behavior of the correlations is quite complicated and that in particular $S(\omega, \mathcal{T})$ and $S(\infty, \mathcal{T})$ do not decouple neither at a finite nor at an infinite observation time. The case (b) is shown in figure 2, panel (b), where $\rho_{\text{BM}}(\omega, \alpha\omega)$ is plotted as a function of $\omega \mathcal{T}$ for several values of α . We observe that $S(\omega, \mathcal{T})$ and $S(\alpha\omega, \mathcal{T})$ are completely correlated within some well-defined region of values of $\omega \mathcal{T}$, and such a correlation drops rapidly to the constant level $2/5$ upon a further increase of $\omega \mathcal{T}$. The size of the window in which $S(\omega, \mathcal{T})$ and $S(\alpha\omega, \mathcal{T})$ are completely correlated increases as α approaches 1, which is not counter-intuitive.

Finally, summarizing our results for the BM and recalling that $\gamma_{\text{BM}}(0, \mathcal{T}) = \sqrt{2}$ and $\gamma_{\text{BM}}(\omega > 0, \mathcal{T} = \infty) = \sqrt{5}/2$ [30], we find that the covariance function of the random amplitude b_ω (see equations (3) and (12)) in the frequency domain is given, as $\mathcal{T} \rightarrow \infty$, by

$$\overline{b_{\omega_1} b_{\omega_2}} = \begin{cases} 3/2, & \text{for } \omega_1 \neq \omega_2, \quad \omega_1 \omega_2 > 0; \\ 7/4, & \text{for } \omega_1 = 0, \quad \omega_2 > 0; \\ 9/4, & \text{for } \omega_1 = \omega_2 > 0; \\ 3, & \text{for } \omega_1 = \omega_2 = 0. \end{cases} \tag{24}$$

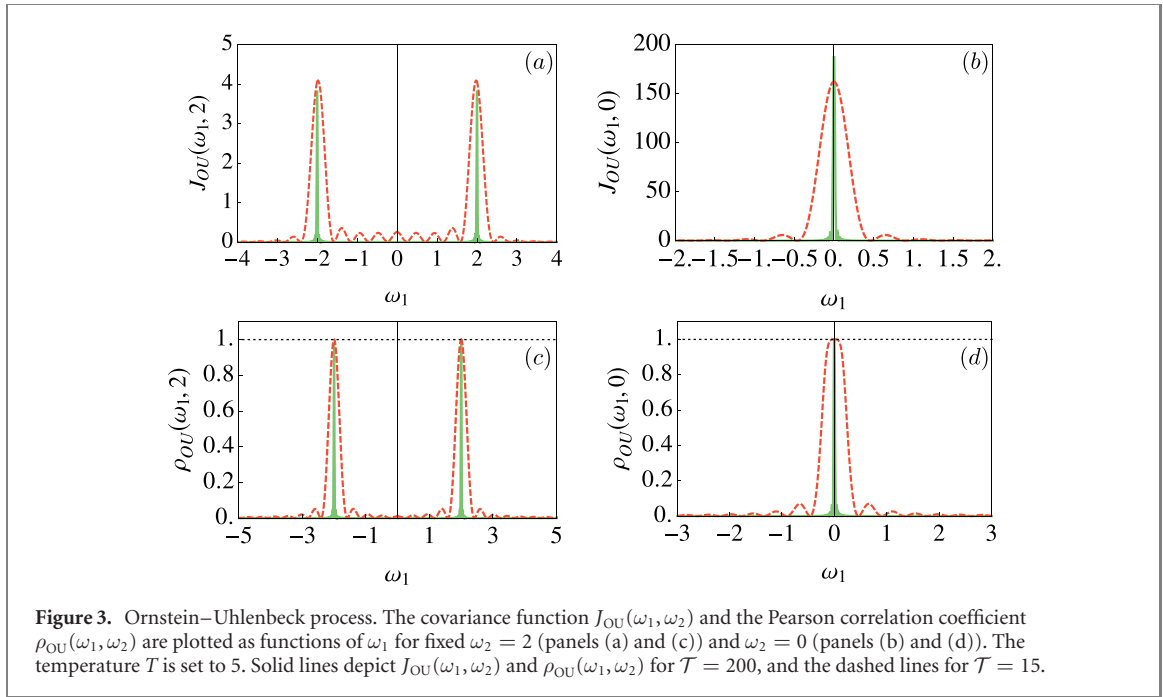
This implies that the b_ω exhibit some degree of correlation for different values of ω .

3.2. Ornstein–Uhlenbeck process

The OU process obeys the Langevin equation

$$\dot{X} = -X + \zeta(t), \tag{25}$$

where $\zeta(t)$ is a Gaussian noise whose properties are defined in equation (14). At variance with the BM, this process approaches a stationary distribution when $t \rightarrow \infty$. The solution of equation (25) for the initial



condition $X(0) = 0$ and a given realization of the noise is given by

$$X(t) = e^{-t} \int_0^t d\tau e^{\tau} \zeta(\tau). \quad (26)$$

Consequently, the two-time correlation function of $X(t)$ for $t_2 \leq t_1$ is given by

$$\overline{X(t_1)X(t_2)} = T[\exp(-(t_1 - t_2)) - \exp(-(t_1 + t_2))]. \quad (27)$$

The correlation function $\overline{X(t_1)X(t_2)}$ for $t_2 \geq t_1$ is obtained by merely interchanging t_2 and t_1 in this relation. Note that, in contrast to the BM whose mean-squared displacement grows without bounds in time, the variance of OU process is bounded. Indeed, setting $t_1 = t_2 = t$ in equation (27), we obtain $\overline{X^2(t)} = T(1 - \exp(-2t))$, and therefore the mean-squared displacement from the origin approaches the constant value T for $t \rightarrow \infty$.

Inserting the expression (27) into equation (9) and performing the integrations, we eventually find a rather lengthy expression for $J_{OU}(\omega_1, \omega_2)$, which holds for arbitrary ω_1, ω_2 , and \mathcal{T} and it is unnecessary to copy here. We show in figure 3 the behavior of $J_{OU}(\omega_1, \omega_2)$ as a function of ω_1 for two values of the frequency ω_2 : $\omega_2 = 2$ and $\omega_2 = 0$ (see panels (a) and (b)). We observe that $J_{OU}(\omega_1, \omega_2)$ behaves differently from the BM case in several aspects. First of all, for $\omega_2 = 2$ the covariance function $J_{OU}(\omega_1, \omega_2)$ exhibits only the peaks at $\omega_1 = \pm\omega_2$, while the peak at $\omega_1 = 0$ is absent. Moreover, the height of the peak at $\omega_1 = \pm\omega_2 \neq 0$ is given by

$$J_{OU}(\omega, \omega) = \frac{4T^2}{(1 + \omega^2)^2} + \frac{4T^2(\omega^2 - 3)}{(1 + \omega^2)^3\mathcal{T}} + \frac{2T^2(1 + 7\omega^2 - \omega^4 + \omega^6)}{\omega^2(1 + \omega^2)^4\mathcal{T}^2} + \frac{2T^2(3\omega^2 - 1)\cos(2\omega\mathcal{T})}{\omega^2(1 + \omega^2)^3\mathcal{T}^2} + \frac{2T^2(\omega^2 - 3)\sin(2\omega\mathcal{T})}{\omega(1 + \omega^2)^3\mathcal{T}^2} + \mathcal{O}(e^{-\mathcal{T}}), \quad (28)$$

where the symbol $\mathcal{O}(e^{-\mathcal{T}})$ signifies that the omitted terms decay exponentially with the observation time. Therefore, the height of the peaks approaches a \mathcal{T} -independent value as $\mathcal{T} \rightarrow \infty$, which decays as the fourth inverse power of the frequency in the limit $\omega \rightarrow \infty$. This is quite similar to the behaviour of $J_{BM}(\omega, \omega)$ (see equation (18)). Note that the limit $\omega \rightarrow 0$ of the expression (28) does not correctly reproduce $J_{OU}(0, 0)$. In fact, the height of the peak in case $\omega_1 = \omega_2 = 0$ must be evaluated by setting $\omega_1 = 0$ and $\omega_2 = 0$ from the very beginning. In doing so, we find that $J_{OU}(0, 0)$ is given by

$$J_{OU}(0, 0) = 8T^2 - \frac{24T^2}{\mathcal{T}} + \frac{18T^2}{\mathcal{T}^2} + \mathcal{O}(e^{-\mathcal{T}}), \quad (29)$$

where the coefficient in front of T^2 is twice what would be obtained directly from equation (28).

We now dwell on the case $\omega_1 \neq \omega_2$. Here, rather lengthy calculations show that $J_{\text{OU}}(\omega_1, \omega_2)$ has the following large- \mathcal{T} asymptotic form:

$$J_{\text{OU}}(\omega_1, \omega_2) = \frac{2T^2 A_{\text{OU}}(\omega_1, \omega_2)}{\mathcal{T}^2} + O(e^{-\mathcal{T}}), \quad (30)$$

where the omitted terms decay, in the leading order, in proportion to $\exp(-\mathcal{T})$, while the decay amplitude $A_{\text{OU}}(\omega_1, \omega_2)$ in the first term on the right-hand-side of equation (30) is given explicitly by

$$\begin{aligned} A_{\text{OU}}(\omega_1, \omega_2) = & \frac{8(\omega_1^2 + \omega_2^2) + (\omega_1^2 - \omega_2^2)^2}{(1 + \omega_1^2)(1 + \omega_2^2)(\omega_1^2 - \omega_2^2)^2} \\ & - \frac{4((1 + \omega_1\omega_2)^2 + \omega_1\omega_2(\omega_1 - \omega_2)^2)}{(1 + \omega_1^2)^2(1 + \omega_2^2)^2(\omega_1 - \omega_2)^2} \cos((\omega_1 - \omega_2)\mathcal{T}) \\ & - \frac{4((1 - \omega_1\omega_2)^2 - \omega_1\omega_2(\omega_1 + \omega_2)^2)}{(1 + \omega_1^2)^2(1 + \omega_2^2)^2(\omega_1 + \omega_2)^2} \cos((\omega_1 + \omega_2)\mathcal{T}) \\ & - \frac{2(3 + \omega_1^2 + \omega_2^2 - \omega_1^2\omega_2^2)}{(1 + \omega_1^2)^2(1 + \omega_2^2)^2} \frac{\sin((\omega_1 - \omega_2)\mathcal{T})}{\omega_1 - \omega_2} \\ & - \frac{2(3 + \omega_1^2 + \omega_2^2 - \omega_1^2\omega_2^2)}{(1 + \omega_1^2)^2(1 + \omega_2^2)^2} \frac{\sin((\omega_1 + \omega_2)\mathcal{T})}{\omega_1 + \omega_2}. \end{aligned} \quad (31)$$

This expression contains the \mathcal{T} -independent first term, while the following ones oscillate with \mathcal{T} .

Therefore, when $\omega_1 \neq \omega_2$ and both are non-vanishing, $J_{\text{OU}}(\omega_1, \omega_2)$ vanishes in the limit $\mathcal{T} \rightarrow \infty$, implying that the random variables $S(\omega_1, \mathcal{T} \rightarrow \infty)$ and $S(\omega_2, \mathcal{T} \rightarrow \infty)$ become statistically independent. Moreover, keeping ω_1 fixed and $\omega_2 \rightarrow \infty$, we observe that $A_{\text{OU}}(\omega_1, \omega_2)$ in equation (31) vanishes as $1/\omega_2^2$, meaning that correlations between $S(\omega_1, \mathcal{T})$ and $S(\omega_2, \mathcal{T})$ also vanish when \mathcal{T} is finite (but large enough to ensure the validity of the asymptotic form in equation (30)) and $|\omega_1 - \omega_2| \rightarrow \infty$. Such a behaviour is markedly different from the one we found for the BM. Finally, we obtain that the covariance function of the random amplitude b_ω (see equation (3)) satisfies in the limit $\mathcal{T} \rightarrow \infty$ the relations

$$\overline{b_{\omega_1} b_{\omega_2}} = \begin{cases} 1, & \text{for } \omega_1 \neq \omega_2, \quad \omega_1, \omega_2 > 0; \\ 1, & \text{for } \omega_1 = 0, \quad \omega_2 > 0; \\ 2, & \text{for } \omega_1 = \omega_2 > 0; \\ 3, & \text{for } \omega_1 = \omega_2 = 0. \end{cases} \quad (32)$$

These values are different from the BM case, except for the case $\omega_1 = \omega_2 = 0$. Notice that this implies that the b_ω for different values of ω are totally uncorrelated.

4. Brownian gyrator

We focus next on the BG model [38], defined as a pair of coupled OU processes $X(t)$ and $Y(t)$, which obey the following system of Langevin equations:

$$\begin{aligned} \dot{X} &= -X + uY + \zeta_x(t), \\ \dot{Y} &= -Y + uX + \zeta_y(t). \end{aligned}$$

Here $\zeta_{x,y}$ are Gaussian zero-mean white noises such that

$$\overline{\zeta_i(t)\zeta_j(t')} = 2T_i\delta_{ij}\delta(t-t'), \quad i, j = x, y, \quad (33)$$

where $\delta_{i,j}$ is the Kronecker delta, while T_x and T_y are the temperatures (measured in units of the Boltzmann constant) of two thermal baths.

Despite its simplicity, the model defined by equation (33) exhibits a rather non-trivial physical behaviour. It was in fact realized in [39] that it represents a minimal model of a heat machine. When $u = 0$, $X(t)$ and $Y(t)$ decouple and form two independent OU processes, leading us back to the case studied in the

previous section 3.2. On the other hand, when $0 < |u| < 1$ and $T_x \neq T_y$, the system eventually reaches a non-equilibrium steady state, characterized by a non-vanishing average rotation frequency in the (X, Y) plane. This explains the name of the model. Various aspects of the BG dynamical behaviour and of its steady-state properties have been studied, see, e.g., [24, 25] and [40–51]. In particular, a non-trivial fluctuation theorem was established by considering the response of the BG to external regular forces, what allowed to define explicitly an effective temperature [46–48]. We also remark that the setting with constant forces exerted on the BG is mathematically identical to the one-dimensional bead-spring model studied via Brownian-dynamics simulations in [52] and analytically in [53, 54]. A generalization of the BG model for a system of two coupled noisy Kuramoto oscillators has been discussed in [55].

Solving equation (33) for the trajectories, with the initial condition $X(0) = Y(0) = 0$, we find that for given realisations of noises $\zeta_x(\tau)$ and $\zeta_y(\tau)$, $X(t)$ and $Y(t)$ are given by

$$\begin{aligned} X(t) &= e^{-t} \int_0^t d\tau e^\tau \cosh(u(t-\tau))\zeta_x(\tau) + e^{-t} \int_0^t d\tau e^\tau \sinh(u(t-\tau))\zeta_y(\tau), \\ Y(t) &= e^{-t} \int_0^t d\tau e^\tau \sinh(u(t-\tau))\zeta_x(\tau) + e^{-t} \int_0^t d\tau e^\tau \cosh(u(t-\tau))\zeta_y(\tau). \end{aligned} \tag{34}$$

We thus obtain the following expressions for the two-time correlation function of the X -component. For $t_1 \geq t_2$ we have

$$\begin{aligned} \overline{X(t_1)X(t_2)} &= \frac{e^{-t_1-t_2}}{2(1-u^2)} \left[\cosh(u(t_1-t_2))(T_y + e^{t_2}(T_x \cosh(t_2) + (3T_x + 2u^2(T_y - T_x)) \sinh(t_2))) \right. \\ &\quad \left. - (T_x + T_y)(\cosh(u(t_1-t_2)) + u(\sinh(u(t_1-t_2)) + e^{-2t_2} \sinh(u(t_1-t_2)))) \right]. \end{aligned} \tag{35}$$

For $t_2 \geq t_1$ we have

$$\begin{aligned} \overline{X(t_1)X(t_2)} &= \frac{e^{-t_1-t_2}}{2(1-u^2)} \left[\cosh(u(t_2-t_1))(T_y + e^{t_1}(T_x \cosh(t_1) + (3T_x + 2u^2(T_y - T_x)) \sinh(t_1))) \right. \\ &\quad \left. - (T_x + T_y)(\cosh(u(t_1+t_2)) + u(\sinh(u(t_1+t_2)) - e^{2t_1} \sinh(u(t_2-t_1)))) \right]. \end{aligned} \tag{36}$$

As one may readily check, the variance $\overline{X^2(t)}$ of the X -component is bounded in the $t \rightarrow \infty$ limit:

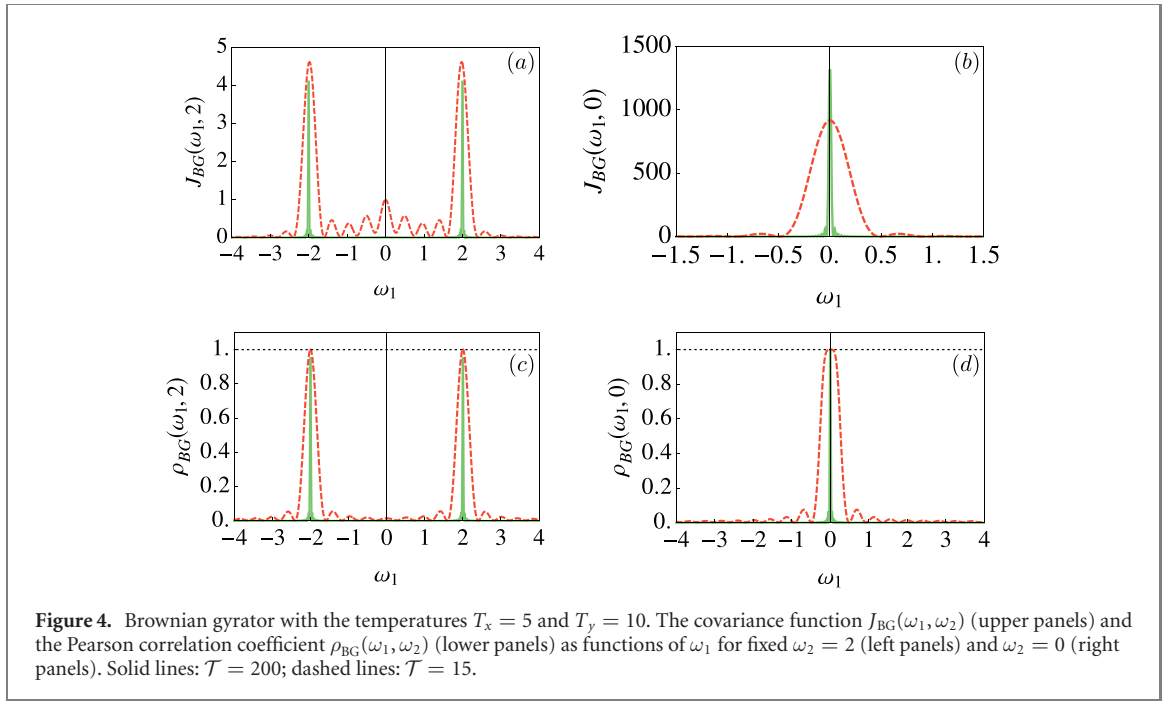
$$\overline{X^2(t)} = \frac{T_x + (u^2/2)(T_y - T_x)}{1 - u^2} + \mathcal{O}(e^{-(1-|u|)t}). \tag{37}$$

The latter expression naturally reduces to the one obtained for the OU process when $u = 0$. A similar expression holds for the Y component.

We now consider the PSD of the X -component of the BG. First, by inserting the expressions (35) and (36) into equations (4) and (7), and evaluating the integrals, we obtain the following large- \mathcal{T} form for the mean PSD of the X -component:

$$\begin{aligned} \mu_x(\omega, \mathcal{T}) &\simeq \frac{2((1+\omega^2)T_x + u^2T_y)}{(\omega^2 + (1-u)^2)(\omega^2 + (1+u)^2)} \\ &\quad - \frac{2\left(\left(\omega^4 + (1+\omega^2)^2 - (u^2 + \omega^2)^2\right)T_x + 2u^2(1-u^2)T_y + 2u^2\omega^2(T_y - T_x)\right)}{(\omega^2 + (1-u)^2)^2(\omega^2 + (1+u)^2)^2} \frac{1}{\mathcal{T}}, \end{aligned} \tag{38}$$

where the omitted terms decay exponentially with \mathcal{T} in the limit $\mathcal{T} \rightarrow \infty$. The symbol \simeq here and henceforth signifies that we consider only the leading terms in the limit $\mathcal{T} \rightarrow \infty$. Next, inserting (35) and (36) into equation (8), we evaluate the covariance function $J_{BG}(\omega_1, \omega_2)$ for arbitrary \mathcal{T} , ω_1 , and ω_2 . Since the obtained expression appears to be too lengthy to be listed explicitly here, we instead show its behavior in figure 4 in the same way as we did it for the OU process. In panels (a) and (b) we present $J_{BG}(\omega_1, \omega_2)$ as function of ω_1 for $\mathcal{T} = 15$ and $\mathcal{T} = 200$, and two fixed values of ω_2 : $\omega_2 = 2$ and $\omega_2 = 0$. We observe that $J_{BG}(\omega_1, \omega_2)$ exhibits essentially the same behaviour as $J_{OU}(\omega_1, \omega_2)$, which was discussed in the previous section, and differs from it only in some details. The covariance function $J_{BG}(\omega_1, \omega_2)$ is an oscillatory



function of ω_1 (and hence, of ω_2) with peaks at $\omega_1 = \pm\omega_2$, which naturally merge into a single peak for $\omega_2 = 0$ (see panel (b)). The height of the peaks, i.e., $J_{BG}(\omega_1 = \omega_2 = \omega)$ (for ω bounded away from zero) is given in the limit $\mathcal{T} \rightarrow \infty$ by

$$J_{BG}(\omega_1 = \omega_2 = \omega) = \frac{\left(2(1-u^2)^2(4(1+\omega^2)T_x + 3u^2T_y)\right)^2 + u^4(\omega^6 + 2(1+u^2)^2)T_y^2}{8(1-u^2)^2(\omega^4 + 2(1+u^2)\omega^2 + (1-u^2)^2)}, \quad (39)$$

i.e., is \mathcal{T} -independent as is its counterpart for the OU process. The difference with the OU case, (apart from the fact that $J_{BG}(\omega, \omega)$ depends on the parameters u , T_x and T_y), is that the height of the peaks vanishes with ω much slower, as the second inverse power of the frequency,

$$J_{BG}(\omega_1 = \omega_2 = \omega) = \frac{u^4 T_y^2}{8(1-u^2)^2 \omega^2} + O\left(\frac{1}{\omega^4}\right), \quad (40)$$

while $J_{OU}(\omega_1 = \omega_2 = \omega) \sim 1/\omega^4$ (see equation (28)). Interestingly enough, the amplitude in this large- ω asymptotic form for the X -component is entirely defined by the temperature of the Y -component of the BG and the coupling parameter u . In turn, for $\omega_2 = 0$, the height of the peak at $\omega_1 = 0$ (see panel (b) in figure 4) approaches in the asymptotic limit $\mathcal{T} \rightarrow \infty$ the following constant value

$$J_{BG}(\omega_1 = \omega_2 = 0) = \frac{8(T_x + u^2 T_y)^2}{(1-u^2)^4}, \quad (41)$$

which reduces to the one in equation (29) when $u = 0$, i.e., the X - and Y -components of the BG decouple.

Lastly, analysing the obtained expression for $J_{BG}(\omega_1, \omega_2)$, we realize that for $\omega_1 \neq \omega_2$ (and both frequencies bounded away from zero) the leading behavior in the large- \mathcal{T} limit is given by

$$J_{BG}(\omega_1, \omega_2) = \frac{A_{BG}(\omega_1, \omega_2)}{\mathcal{T}^2} + o\left(\frac{1}{\mathcal{T}^2}\right), \quad (42)$$

where the omitted sub-leading terms decay as $\exp(-(1-|u|)\mathcal{T})$, and $A_{BG}(\omega_1, \omega_2)$ is a \mathcal{T} -independent amplitude which is a rather complicated function of ω_1 and ω_2 , that we prefer not to show here. Therefore, in the leading in \mathcal{T} order and for $\omega_1 \neq \omega_2$ the covariance function $J_{BG}(\omega_1, \omega_2)$ vanishes as a power law, in proportion to the second inverse power of the observation time. We note, as well, that $A_{BG}(\omega_1, \omega_2)$ vanishes when either of the frequencies is kept fixed while the other one tends to infinity. In particular, for ω_2 fixed and $\omega_1 \rightarrow \infty$, we find

$$A_{\text{BG}}(\omega_1, \omega_2) = \frac{4(T_x + u^2 T_y)^2 + \omega_2^2 (2T_x + u^2(T_y - T_x))^2}{2(1 - u^2)^2 (\omega_2^2 + (1 - u)^2) (\omega_2^2 + (1 + u)^2)} \frac{1}{\omega_1^2} + O\left(\frac{1}{\omega_1^4}\right), \quad (43)$$

meaning that $S(\omega_1, \mathcal{T})$ and $S(\omega_2, \mathcal{T})$ become statistically independent when either $\mathcal{T} \rightarrow \infty$ or when $|\omega_1 - \omega_2| \rightarrow \infty$. Such a behaviour is identical to the one which we observed for the OU process. Moreover, the covariance function $\overline{b_{\omega_1} b_{\omega_2}}$ has exactly the same form as the one of the OU process, equation (32).

In reference [35] the joint distribution of the PSD for X and Y , for the same values of ω and \mathcal{T} has been evaluated.

5. Fractional Brownian motion

We finally consider the FBM [56]. This is a Gaussian process with zero mean and covariance function

$$\overline{X(t_1)X(t_2)} = D(t_1^{2H} + t_2^{2H} - |t_1 - t_2|^{2H}), \quad (44)$$

where the *Hurst index* H is a real number such that $0 < H < 1$. Notice that the FBM is an H -parameterised family of anomalous diffusion processes (except for the case $H = 1/2$, when one recovers the standard BM with independent increments). For $H < 1/2$, the process is sub-diffusive as one can readily infer from equation (44) by setting $t_1 = t_2 = t$ to find that the mean-squared displacement obeys $\overline{X^2(t)} = 2D t^{2H}$, where $2H < 1$. One can show with little effort that the increments of the process in this case have negative long-ranged correlations. On the contrary, for $H > 1/2$ the exponent $2H$ exceeds unity and one observes a super-diffusive behaviour. In this latter case the increments have positive long-ranged correlations. Therefore, one naturally expects for such a family of anomalous diffusion processes a richer behaviour than the one discussed in previous sections.

5.1. Sub-diffusive fractional Brownian motion

We start with the case of sub-diffusion, defined by a value of H satisfying $0 < H < 1/2$. In this case we take advantage of the fact that for $H = 1/4$ we can obtain an explicit, albeit lengthy, expression of the covariance function $J_{\text{FBM}}(\omega_1, \omega_2)$. We checked that the behavior for different values of H in this range, obtained by numerical integration of equation (8), is qualitatively similar. Figure 5 shows the covariance function $J_{\text{FBM}}(\omega_1, \omega_2)$ and the Pearson correlation coefficient $\rho_{\text{FBM}}(\omega_1, \omega_2)$ for $H = 1/4$ as functions of ω_1 for two fixed values of ω_2 : $\omega_2 = 2$ (panels (a) and (c)) and $\omega_2 = 0$ (panels (b) and (d)), and for two values of the observation time, namely $\mathcal{T} = 200$ (solid green curve) and $\mathcal{T} = 15$ (dashed red curve). We observe that $J_{\text{FBM}}(\omega_1, \omega_2)$ exhibits a different behavior from the cases examined so far. Here, in panel (a), the peaks at $\omega_1 = \pm\omega_2$ are much more pronounced than for the BM, and also the central peak at $\omega_1 = 0$ (and $\omega_2 = 2$) appears to diverge with the observation time, what did not happen for the OU process and for the BG model. Indeed, we find (see appendix A) that for $\omega_1 = 0$, and for $(\omega_2 \mathcal{T}) \rightarrow \infty$ (i.e., for either fixed ω_2 and $\mathcal{T} \rightarrow \infty$, or fixed \mathcal{T} and $\omega_2 \rightarrow \infty$), the covariance function $J_{\text{FBM}}(0, \omega)$ obeys

$$J_{\text{FBM}}(0, \omega) \simeq \frac{2D^2 \mathcal{T}^{4H}}{\omega^2}. \quad (45)$$

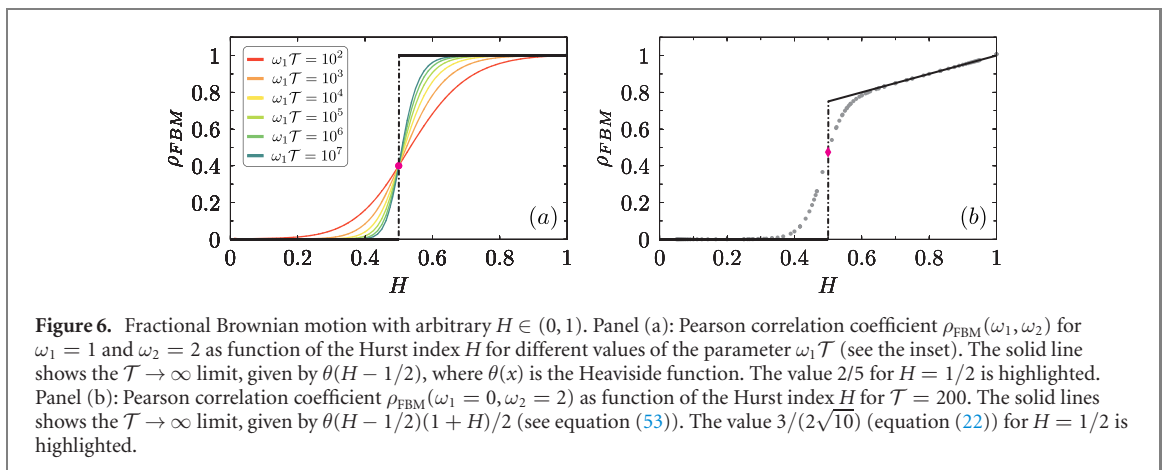
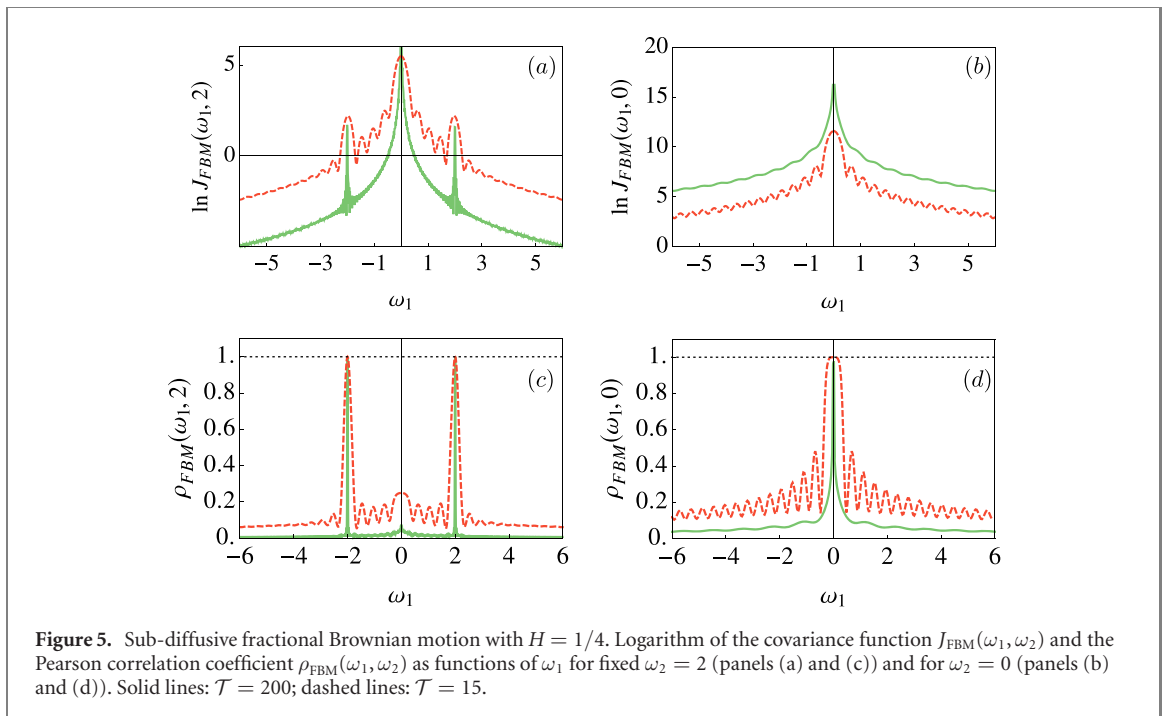
This asymptotic form holds for arbitrary values of H , i.e., for sub-diffusion, super-diffusion, and also for the Brownian case with $H = 1/2$ (see equation (19)). Correction terms to the asymptotic form in equation (45) are shown in appendix A. Interestingly, the ω^{-2} dependence on the frequency ω in equation (45) seems to hold for all the processes studied here. The \mathcal{T} -dependence is, of course, quite different for the processes with a bounded variance (the OU process and the BG model) and for the sub-diffusive FBM for which the variance exhibits an unbounded growth.

Next, on panel (b) of figure 5 we present the covariance function $J_{\text{FBM}}(\omega_1, \omega_2 = 0)$ for $\omega_2 = 0$. We observe that, qualitatively, the behaviour appears similar to the ones encountered in all our above analyses, i.e., $J_{\text{FBM}}(\omega_1, \omega_2 = 0)$ has a single peak at $\omega_1 = 0$. The height of this peak is found analytically to be given by

$$J_{\text{FBM}}(0, 0) = \frac{2D^2 \mathcal{T}^{2+4H}}{(1+H)^2}. \quad (46)$$

This expression is also valid for arbitrary H (see [31] and appendix A). In particular, setting $H = 1/2$ (and hence, $D = T$), we recover our previous equation (20). Since $J_{\text{FBM}}(0, 0)$ is the squared area under the $X(t)$ curve divided by \mathcal{T} , we find quite naturally that it diverges for the FBM as for the BM, at variance with the bounded processes (OU and BG).

Conversely, for sub-diffusive FBM the behaviour of the Pearson correlation coefficient is strikingly different from what we have found for the BM and, in fact, appears to be closer to what we have found for



the OU process and for the BG model. Indeed, we observe in panels (c) and (d) of figure 5 that $\rho_{\text{FBM}}(\omega_1, \omega_2)$ for $H = 1/4$ tends to zero as $\mathcal{T} \rightarrow \infty$, both when $\omega_1 \neq \omega_2$ (and both frequencies are not equal to zero) and when $\omega_2 = 0$ and $\omega_1 \neq 0$. This implies, of course, that the amplitude b_ω in equation (3) is totally uncorrelated for different values of ω in this limit. Furthermore, in figure 6 we show that this is indeed the case for arbitrary H in the sub-diffusive regime: $\rho_{\text{FBM}}(\omega_1, \omega_2)$ with $\omega_1 \neq \omega_2$ vanishes as \mathcal{T} grows for any $H < 1/2$ (see panel (a)) and also $\rho_{\text{FBM}}(\omega_1 = 0, \omega_2 > 0)$ is close to zero when \mathcal{T} is large (see panel (b)).

Below we define the rate at which $\rho_{\text{FBM}}(\omega_1, \omega_2)$ vanishes for the sub-diffusive FBM in the limit $\mathcal{T} \rightarrow \infty$ (see appendix A for the details of intermediate calculations). Suppose first that $\omega_1 = \omega > 0$ and $\omega_2 = 0$. In this special case the analytical calculations are much simpler than for arbitrary fixed ω_2 . We recall that $\rho_{\text{FBM}}(\omega, 0)$ is formally defined by (see equation (11))

$$\rho_{\text{FBM}}(\omega, 0) = \frac{J_{\text{FBM}}(\omega, 0)}{\sqrt{J_{\text{FBM}}(\omega, \omega)J_{\text{FBM}}(0, 0)}}, \quad (47)$$

where the large- \mathcal{T} asymptotic form of $J_{\text{FBM}}(\omega, 0)$ is given in equation (45), while $J_{\text{FBM}}(0, 0)$ is defined in equation (46). In turn, we notice that $J_{\text{FBM}}(\omega, \omega)$ is simply the variance of a single-trajectory PSD of a sub-diffusive FBM. This quantity has been previously determined in [31] for arbitrary $H \in (0, 1)$ and is given by

$$J_{\text{FBM}}(\omega, \omega) = 4D^2 \left(\frac{c_H^2}{\omega^{2+4H}} + \frac{2c_H}{\omega^{3+2H}\mathcal{T}^{1-2H}} + \frac{2}{\omega^4\mathcal{T}^{2-4H}} \right), \tag{48}$$

where $c_H = \Gamma(1 + 2H) \sin(\pi H)$. The expression (48) is valid for arbitrary $\omega > 0$ and sufficiently large \mathcal{T} . Noticing that for $H < 1/2$ the first term in equation (48) defines the dominant large- \mathcal{T} behaviour and combining it with equations (45) and (46), we therefore conclude that for a sub-diffusive FBM the Pearson correlation coefficient $\rho_{\text{FBM}}(\omega, 0)$ vanishes as a power-law when $\mathcal{T} \rightarrow \infty$ as

$$\rho_{\text{FBM}}(\omega, 0) \simeq \frac{1 + H}{\sqrt{2}c_H} \frac{1}{(\omega\mathcal{T})^{1-2H}}. \tag{49}$$

Here, two comments are in order. First, as shown in appendix A (see equation (A.7)), the asymptotic form in equation (45) defines the dominant behaviour in the limit when (sufficiently large) \mathcal{T} is fixed, while $\omega \rightarrow \infty$. Similarly, in this case the dominant large- ω behaviour of the variance in equation (48) is defined by the first term. As a consequence, the asymptotic form in equation (49) describes as well the behaviour of the Pearson coefficient in the limit $\omega \rightarrow \infty$ at fixed sufficiently large \mathcal{T} . We therefore conclude that, similarly to the OU process and the BG model, for sub-diffusive FBM, i.e., for any $H \in (0, 1/2)$, the correlations between $S(0, \mathcal{T})$ and $S(\omega, \mathcal{T})$ vanish when either ω is fixed and $\mathcal{T} \rightarrow \infty$, or when \mathcal{T} is fixed and $\omega \rightarrow \infty$. Second, we note that the limit of expression (49) for $H \rightarrow 1/2$ yields an incorrect value. Indeed, for $H = 1/2$ the Pearson coefficient in equation (49) becomes independent of ω and \mathcal{T} , but the numerical value is wrong. The point is that in order to recover our equation (22), we have to take into account all three terms in equation (48). This implies that the case $H = 1/2$ is singular.

We consider at last the behaviour in a more general case when $\omega_1 \neq \omega_2 > 0$. Relegating the quite tedious calculations to appendix A, we find that in the leading order in the limit $\mathcal{T} \rightarrow \infty$, the covariance function $J_{\text{FBM}}(\omega_1, \omega_2)$ is given by

$$J_{\text{FBM}}(\omega_1, \omega_2) \simeq \frac{8D^2\mathcal{T}^{4H-2}}{\omega_1^2\omega_2^2}, \tag{50}$$

an expression that holds for any $H \in (0, 1)$. Taking into account equation (48), we obtain

$$\rho_{\text{FBM}}(\omega_1, \omega_2) \simeq \frac{2}{c_H^2(\omega_1\omega_2)^{1-2H}\mathcal{T}^{2-4H}}. \tag{51}$$

Hence, in this more general case $\rho_{\text{FBM}}(\omega_1, \omega_2)$ also vanishes as $\mathcal{T} \rightarrow \infty$, and the decay is faster than when either of the frequencies is equal to zero (see equation (49)).

Summarizing, for a sub-diffusive FBM the two-frequency correlation function in equation (12) obeys, in the limit $\mathcal{T} \rightarrow \infty$,

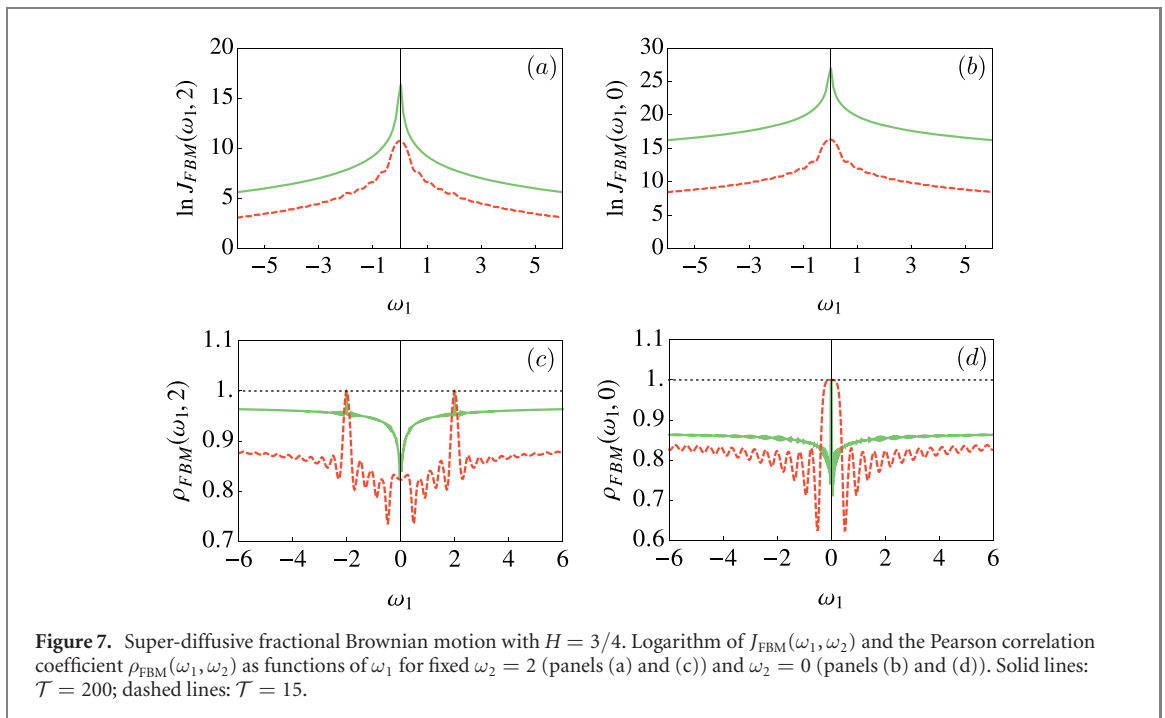
$$\overline{b_{\omega_1} b_{\omega_2}} = \begin{cases} 1, & \text{for } \omega_1 \neq \omega_2; \quad \omega_1, \omega_2 > 0; \\ 1, & \text{for } \omega_1 = 0, \omega_2 > 0; \\ 2, & \text{for } \omega_1 = \omega_2 \neq 0; \\ 3, & \text{for } \omega_1 = \omega_2 = 0. \end{cases} \tag{52}$$

This implies again that for $\omega_1 \neq \omega_2$ the b_ω are totally uncorrelated.

5.2. Super-diffusive fractional Brownian motion

We turn finally to super-diffusive FBM, i.e., to the case with $H > 1/2$. We again exploit the fact that an explicit form of $J_{\text{FBM}}(\omega_1, \omega_2)$ is available for the special value $H = 3/4$. In figure 7 we plot $J_{\text{FBM}}(\omega_1, \omega_2)$ for this value of H as a function of ω_1 for $\omega_2 = 2$ (panel (a)) and $\omega_2 = 0$ (panel (b)), as well as the corresponding Pearson coefficient $\rho_{\text{FBM}}(\omega_1, \omega_2)$ (panels (c) and (d)). However, we verified that the curves exhibit essentially the same behaviour for any value of H in the super-diffusive regime.

We find that the behaviour in the super-diffusive case appears to be *qualitatively* different, as compared to the previous situations. We observe in particular that $J(\omega_1, \omega_2 = 2)$ in panel (a) of figure 7 grows uniformly as \mathcal{T} grows, while in the previous case it either decreased as \mathcal{T} increased (for the OU process, the BG model and sub-diffusive FBM), or reached a \mathcal{T} -independent limit, as for the BM (except for the vicinity of $\omega_1 = 0$). Moreover, the peaks at $\omega_1 = \pm 2$ are less pronounced than in the above studied situations and become almost indistinguishable from the base curve for longer observation times. This apparently signals that the correlations between $S(\omega_1, \mathcal{T})$ and $S(\omega_2, \mathcal{T})$ become very strong for any different values of ω_1 and ω_2 . Of course, this is not totally surprising, because of the strongly correlated increments of the parental process. On the other hand, $J_{\text{FBM}}(\omega_1, 0)$ (see panel (b) in figure 7) behaves very similarly to the BM or the sub-diffusive FBM.



The behaviour of the Pearson correlation coefficient $\rho_{\text{FBM}}(\omega_1, \omega_2 = 2)$ on panel (c) of figure 7 also differs qualitatively from what we have previously observed in two aspects: (i) while there still exist two peaks at $\omega_1 = \pm 2$, there is no peak at $\omega_1 = 0$ and there is instead a dip, and (ii) $\rho_{\text{FBM}}(\omega_1, \omega_2 = 2)$ raises towards higher values upon an increase of \mathcal{T} (except in the vicinity of $\omega_1 = 0$). Such an increase with increasing \mathcal{T} is also apparent in panel (d). The levels which the curves attain for $\mathcal{T} = 200$ are, however, rather different.

To interpret this behavior, we start by dwelling on $J_{\text{FBM}}(\omega_1, \omega_2 = 0)$, which defines the value of the covariance function at the location of the dip on panel (c) and on its behavior depicted on the panel (d). We focus first on the limit $\mathcal{T} \rightarrow \infty$ with ω_1 kept fixed. In this limit, the dominant contribution to $J_{\text{FBM}}(\omega, \omega)$ in equation (48) is provided by the third term in the brackets, while the first sub-dominant correction is given by the second term. The first term is irrelevant, unlike for the case of sub-diffusion, for which it plays the dominant role. Recalling the expressions (45) and (46), we find that the Pearson correlation coefficient admits the following asymptotic form for large \mathcal{T} :

$$\rho_{\text{FBM}}(\omega_1, 0) = \frac{H + 1}{2} \left(1 - \frac{c_H}{2(\omega_1 \mathcal{T})^{2H-1}} + o\left(\frac{1}{\mathcal{T}^{2H-1}}\right) \right). \tag{53}$$

Therefore, $\rho_{\text{FBM}}(\omega_1, 0)$ indeed increases as \mathcal{T} grows, saturating at the constant value $(H + 1)/2$. Such a behaviour is clearly seen on panel (b) of figure 6, in which we plot $\rho_{\text{FBM}}(0, \omega_2 = 2)$ as function of H for a sufficiently large observation time ($\mathcal{T} = 200$), as well as the leading term in equation (53). We note that expression (53) yields an incorrect value in the limit $H \rightarrow 1/2$. We thus have a discontinuity at $H = 1/2$: a drop from the value $3/4$ predicted by equation (53) when we extrapolate H to $1/2$, to the smaller actual value $3/(2\sqrt{10}) \approx 0.474$ (see equation (22)).

Next, we look at the correlations of $S(\omega_1, \mathcal{T})$ and $S(0, \mathcal{T})$, in the limit $\omega_1 \rightarrow \infty$ with \mathcal{T} kept fixed and sufficiently large to ensure the validity of equation (48). Inspecting equation (48), we obtain that the leading behaviour in this limit is provided by the third term in the brackets and the first sub-dominant correction comes from the second term. This straightforwardly implies that $\rho_{\text{FBM}}(\omega_1, 0)$ in this limit obeys equation (53). Thus the Pearson correlation coefficient saturates at the constant value $(1 + H)/2$ and correlations do not decouple completely. Such a behaviour is apparent in figure 6 (panel (b)).

Lastly, we turn to the more general case when $\omega_1 \neq \omega_2$, both non-zero. Taking advantage of equations (48) and (50), we arrive at

$$\lim_{\mathcal{T} \rightarrow \infty} \rho_{\text{FBM}}(\omega_1, \omega_2) = 1. \tag{54}$$

This means that for a super-diffusive FBM the variables $S(\omega_1, \mathcal{T})$ and $S(\omega_2, \mathcal{T})$ become *completely correlated* in the limit $\mathcal{T} \rightarrow \infty$.

Summarizing, we have, in the limit $\mathcal{T} \rightarrow \infty$,

$$\overline{b_{\omega_1} b_{\omega_2}} = \begin{cases} 3, & \text{for } \omega_1 \neq \omega_2; \quad \omega_1, \omega_2 > 0; \\ 2 + H, & \text{for } \omega_1 = 0, \omega_2 > 0; \\ 3, & \text{for } \omega_1 = \omega_2 \neq 0; \\ 3, & \text{for } \omega_1 = \omega_2 = 0. \end{cases} \quad (55)$$

We thus have complete correlations among the b_ω , when $\omega \neq 0$, and a partial one when one of the ω vanishes. We can therefore conclude that the correlations of b_ω are a powerful probe to distinguish between the sub-diffusive, diffusive and super-diffusive cases of the anomalous diffusions.

6. Conclusions

In conclusion, we examined the correlations of the reduced spectral density $b_\omega = S(\omega, \mathcal{T})/\mu(\omega, \mathcal{T})$ for a class of Gaussian random processes, where $S(\omega, \mathcal{T})$ is the spectral density of a single trajectory $X(t)$ of the process, equation (4), ω is the frequency, \mathcal{T} is the observation time, and $\mu(\omega, \mathcal{T}) = \overline{S(\omega, \mathcal{T})}$ is the average of $S(\omega, \mathcal{T})$ over all realizations of the process. It was shown in previous works that for a number of different classes of Gaussian stochastic processes, the spectral density $S(\omega, \mathcal{T})$ is a random variable whose probability distribution depends on $S(\omega, \mathcal{T})$ and $\mu(\omega, \mathcal{T})$ only in the combination $b_\omega = S(\omega, \mathcal{T})/\mu(\omega, \mathcal{T})$. (The resulting distribution depends moreover on ω only via the coefficient of variation $\gamma(\omega, \mathcal{T})$.) We have therefore looked at b_ω as an ω -dependent random quantity. Looking at the behavior of this quantity for different values of ω and for different cases, we have shown that the values of b_ω can be either fully uncorrelated (e.g., for the Ornstein–Uhlenbeck process, for the BG, and for the subdiffusive Brownian motion), partially correlated (e.g., for the ordinary, diffusive Brownian motion) or totally correlated (e.g., for superdiffusive Brownian motion, when both frequencies are non-vanishing). Therefore b_ω can be used as a sensitive probe of the nature of the process, that is available upon inspection of a single trajectory, provided the observation time \mathcal{T} is large enough. It can thus supplement in this role the coefficient of variation γ . Indeed, it was suggested in [31] to use γ as a criterion that permits to distinguish between different kinds of Gaussian processes. This requires, however, to evaluate either the large- ω asymptotical behaviour of γ in case of sub-diffusion and diffusion, or its ageing properties (i.e., its \mathcal{T} -dependence) for superdiffusion, what may be somewhat difficult to access. Thus using b_ω appears advantageous, because it does not require to evaluate the asymptotical behavior, and the values of the frequencies can be arbitrarily chosen. In particular, if we look at the $\overline{b_\omega b_{\omega'}}$ correlation function when one of the frequencies vanish in the super-diffusive FBM case, we are able to extract the value of the Hurst parameter H . As a perspective, we envisage to consider another exactly solvable family of anomalous Gaussian processes—the so-called scaled Brownian motion (see, e.g., [33])—in order to verify our general conclusions and moreover, to check whether an analysis of the frequency–frequency correlations permits to distinguish between different kinds of anomalous diffusions.

There remains, of course, the challenging problem of extending this kind of analysis to non-Gaussian processes.

Acknowledgments

The authors wish to thank Eli Barkai and Sergio Ciliberto for many helpful discussions. AS and LP acknowledge the warm hospitality of LPTMC, Sorbonne Université, respectively, in October–December 2021 and in April 2022. AS acknowledges FWF Der Wissenschaftsfonds for funding through the Lise-Meitner Fellowship (Grant No. M3300-N) and the Department Theory of Inhomogeneous Condensed Matter at the Max-Planck-Institute for Intelligent Systems (Stuttgart) for financial support. LR acknowledges the support of Italian National Group of Mathematical Physics (GNFM) of INDAM, and of Ministero dell’Istruzione e dell’Università e della Ricerca (MIUR), Italy, Grant No. E11G18000350001 ‘Dipartimenti di Eccellenza 2018–2022’.

Data availability statement

The data that support the findings of this study are available upon reasonable request from the authors.

Appendix A. Analytical results for FBM

A.1. Covariance function $J_{\text{FBM}}(\mathbf{0}, \omega)$

We take advantage of the representation of the covariance function of the FBM with arbitrary H in the integral form (see [57]), in which the kernel has a convenient factorised dependence on t_1 and t_2 :

$$t_1^{2H} + t_2^{2H} - |t_1 - t_2|^{2H} = \frac{2c_H}{\pi} \int_0^\infty \frac{dz}{z^{2H+1}} [\sin(zt_1) \sin(zt_2) + (1 - \cos(zt_1))(1 - \cos(zt_2))], \quad (\text{A.1})$$

where

$$c_H = \Gamma(2H + 1) \sin(\pi H). \quad (\text{A.2})$$

Inserting this expression into the definition of $J(\omega_1, \omega_2)$, we perform the integrations over the time variables, and eventually, over z . In doing so, we find that $J(0, \omega)$ is given by

$$J_{\text{FBM}}(0, \omega) = D^2 \mathcal{T}^{2+4H} \mathcal{J}_H(w), \quad w = \omega \mathcal{T}, \quad (\text{A.3})$$

where $\mathcal{J}_H(w)$ is the following function of the dimensionless variable w only:

$$\mathcal{J}_H(w) = \frac{1}{2(1+H)^2(1+2H)^4} \left[\frac{w^2}{(2H+3)^2} \mathcal{K}_1^2(w, H) + \mathcal{K}_2^2(w, H) \right]. \quad (\text{A.4})$$

In this expression, one has

$$\begin{aligned} \mathcal{K}_1(w, H) = & (2H+3) {}_1F_2\left(1; H+\frac{3}{2}, H+2; -\frac{w^2}{4}\right) - 2 {}_1F_2\left(2; H+2, H+\frac{5}{2}; -\frac{w^2}{4}\right) \\ & - (1+2H)(4H^2+8H+3) {}_1F_2\left(H+1; \frac{3}{2}, H+2; -\frac{w^2}{4}\right) \\ & + 2(1+H)(1+2H) {}_1F_2\left(H+\frac{3}{2}; \frac{3}{2}, H+\frac{5}{2}; -\frac{w^2}{4}\right) \\ & - 2(1+H)(1+2H)(2H+3) \frac{(1-\cos(w))}{w^2}, \end{aligned} \quad (\text{A.5})$$

and

$$\begin{aligned} \mathcal{K}_2(w, H) = & -2(H+1) {}_1F_2\left(1; H+1, H+\frac{3}{2}; -\frac{w^2}{4}\right) \\ & - {}_1F_2\left(H+1; \frac{1}{2}, H+2; -\frac{w^2}{4}\right) \\ & - 2H {}_1F_2\left(H+1; \frac{1}{2}, H+2; -\frac{w^2}{4}\right) \\ & + {}_2F_3\left(1, \frac{3}{2}; \frac{1}{2}, H+\frac{3}{2}, H+2; -\frac{w^2}{4}\right) \\ & + 2(2H^2+3H+1) {}_1F_2\left(H+\frac{1}{2}; \frac{1}{2}, H+\frac{3}{2}; -\frac{w^2}{4}\right) \\ & + 2(H^2+3H+1) \frac{\sin(w)}{w}, \end{aligned} \quad (\text{A.6})$$

where ${}_1F_2$ and ${}_2F_3$ are hypergeometric functions. The expression (A.3) is valid for arbitrary $H \in (0, 1)$ and for arbitrary values of \mathcal{T} and ω . In particular, for $\omega = 0$ it reduces to expression (46).

We next consider the large- w behaviour of $J_{\text{FBM}}(0, \omega)$ in equation (A.3), which is realised when either ω is fixed and \mathcal{T} tends to infinity, or alternatively, \mathcal{T} is fixed but $\omega \rightarrow \infty$. Expanding the hypergeometric functions in the limit when $w = (\omega \mathcal{T}) \rightarrow \infty$, we find

$$\begin{aligned} J_{\text{FBM}}(0, \omega) = & \frac{2D^2 \mathcal{T}^{4H}}{\omega^2} \left[\left(\sin(w) - \frac{c_H}{w^{2H}} - \frac{1 + (1-2H)\cos(w)}{w} + \mathcal{O}\left(\frac{1}{w^{2H+1}}\right) \right)^2 \right. \\ & \left. + \left(\cos(w) - \frac{c_H \cot(w)}{w^{2H}} + \frac{(1-2H)\sin(w)}{w} + \mathcal{O}\left(\frac{1}{w^{2H+1}}\right) \right)^2 \right], \end{aligned} \quad (\text{A.7})$$

where c_H is defined in equation (A.2). This expression is dominated by the first terms in the parentheses, that oscillate as functions of w . We thus arrive at the asymptotic form in equation (45). Notice that this expression is valid for any H such that $0 < H < 1$. The finite- w corrections to the leading behaviour in equation (45) are however different in the cases $H < 1/2$, $H = 1/2$ or $H > 1/2$. Indeed, in case of sub-diffusion, the dominant correction terms is given by the second terms in brackets in equation (A.7), while in the super-diffusive case is given by the third terms.

A.2. Large- \mathcal{T} asymptotic behaviour of the covariance function $J_{\text{FBM}}(\omega_1, \omega_2)$

Here we discuss the large- \mathcal{T} behaviour of the covariance function $J_{\text{FBM}}(\omega_1, \omega_2)$ in the more general case when $\omega_1 \neq \omega_2$ and both frequencies are non-vanishing. We start by appropriately rescaling the integration variables in equation (9) to get, e.g., for W_{cc} , the following representation

$$\frac{W_{\text{cc}}(\omega_1, \omega_2; \mathcal{T})}{D\mathcal{T}^{2H+1}} = \int_0^1 d\tau_1 \cos(\omega_1 \mathcal{T} \tau_1) \int_0^1 d\tau_2 (\tau_1^{2H} + \tau_2^{2H} - |\tau_1 - \tau_2|^{2H}) \cos(\omega_2 \mathcal{T} \tau_2). \tag{A.8}$$

Similar expression can be obtained for W_{cs} , W_{cs} and W_{ss} and will differ from the one in equation (A.8) only by the sine and cosine factors. The integrals corresponding to the first and the second terms in the covariance function can be performed analytically and give, in the leading in the limit order for $\mathcal{T} \rightarrow \infty$,

$$\begin{aligned} & \int_0^1 d\tau_1 \left\{ \begin{array}{l} \cos(\omega_1 \mathcal{T} \tau_1) \\ \sin(\omega_1 \mathcal{T} \tau_1) \end{array} \right\} \int_0^1 d\tau_2 \tau_2^{2H} \left\{ \begin{array}{l} \cos(\omega_2 \mathcal{T} \tau_2) \\ \sin(\omega_2 \mathcal{T} \tau_2) \end{array} \right\} \\ &= \left\{ \begin{array}{l} \sin(\omega_1 \mathcal{T}) \\ 1 - \cos(\omega_1 \mathcal{T}) \end{array} \right\} \left\{ \begin{array}{l} \sin(\omega_2 \mathcal{T}) \\ -\cos(\omega_2 \mathcal{T}) \end{array} \right\} \frac{1}{\omega_1 \omega_2 \mathcal{T}^2} + \mathcal{O}\left(\frac{1}{\mathcal{T}^3}\right). \end{aligned} \tag{A.9}$$

This asymptotic expression is valid for any $0 < H < 1$. The analysis of the integrals involving the third, non-local term in the covariance of the FBM is a bit more delicate and we first would like to cast it in a more transparent form. To this end, we expand both cosine functions in powers of τ_1 and τ_2 , perform the integrals, and then re-sum the series. In doing so, we get

$$\begin{aligned} & \int_0^1 d\tau_1 \cos(\omega_1 \mathcal{T} \tau_1) \int_0^1 d\tau_2 |\tau_1 - \tau_2|^{2H} \cos(\omega_2 \mathcal{T} \tau_2) \\ &= \frac{\Gamma(2H + 1)}{(\omega_2 \mathcal{T})^{2H+2}} \int_0^{\omega_2 \mathcal{T}} u^{2H+1} du \cos\left(\frac{\omega_1}{\omega_2} u\right) E_{2,2(H+1)}(-u^2) \\ &+ \frac{\Gamma(2H + 1)}{(\omega_1 \mathcal{T})^{2H+2}} \int_0^{\omega_1 \mathcal{T}} u^{2H+1} du \cos\left(\frac{\omega_2}{\omega_1} u\right) E_{2,2(H+1)}(-u^2), \end{aligned} \tag{A.10}$$

where

$$E_{2,2(H+1)}(u) = \sum_{k=0}^{\infty} \frac{u^k}{\Gamma(2k + 2(H + 1))} \tag{A.11}$$

is the Mittag–Leffler function, whose behaviour is well-documented [58]. In a similar way, we obtain the following results:

$$\begin{aligned} & \int_0^1 d\tau_1 \cos(\omega_1 \mathcal{T} \tau_1) \int_0^1 d\tau_2 |\tau_1 - \tau_2|^{2H} \sin(\omega_2 \mathcal{T} \tau_2) \\ &= \frac{\Gamma(2H + 1)}{(\omega_2 \mathcal{T})^{2H+2}} \int_0^{\omega_2 \mathcal{T}} u^{2H+2} du \cos\left(\frac{\omega_1}{\omega_2} u\right) E_{2,2H+3}(-u^2); \end{aligned} \tag{A.12}$$

$$\begin{aligned} & \int_0^1 d\tau_1 \sin(\omega_1 \mathcal{T} \tau_1) \int_0^1 d\tau_2 |\tau_1 - \tau_2|^{2H} \cos(\omega_2 \mathcal{T} \tau_2) \\ &= \frac{\Gamma(2H + 1)}{(\omega_1 \mathcal{T})^{2H+2}} \int_0^{\omega_1 \mathcal{T}} u^{2H+2} du \cos\left(\frac{\omega_2}{\omega_1} u\right) E_{2,2H+3}(-u^2); \end{aligned} \tag{A.13}$$

$$\begin{aligned} & \int_0^1 d\tau_1 \sin(\omega_1 \mathcal{T} \tau_1) \int_0^1 d\tau_2 |\tau_1 - \tau_2|^{2H} \sin(\omega_2 \mathcal{T} \tau_2) \\ &= \frac{\Gamma(2H + 1)}{(\omega_1 \mathcal{T})^{2H+2}} \int_0^{\omega_1 \mathcal{T}} u^{2H+2} du \sin\left(\frac{\omega_2}{\omega_1} u\right) E_{2,2H+3}(-u^2) \\ &+ \frac{\Gamma(2H + 1)}{(\omega_2 \mathcal{T})^{2H+2}} \int_0^{\omega_2 \mathcal{T}} u^{2H+2} du \sin\left(\frac{\omega_1}{\omega_2} u\right) E_{2,2H+3}(-u^2). \end{aligned} \tag{A.14}$$

We now turn to the analysis of the leading large- \mathcal{T} asymptotic behaviour of expressions (A.12) to (A.14). To this end, we first note that the leading large- u asymptotic behaviour of the Mittag–Leffler function obeys

$$E_{2,\beta}(-u^2) \simeq \frac{1}{\Gamma(\beta-2)} \frac{1}{u^2}. \quad (\text{A.15})$$

Consequently, the integral which enters equation (A.12) diverges on the upper terminal of integration in the super-diffusive case, and converges to a finite value when $\mathcal{T} \rightarrow \infty$ in the sub-diffusive case. This yields

$$\begin{aligned} & \int_0^1 d\tau_1 \cos(\omega_1 \mathcal{T} \tau_1) \int_0^1 d\tau_2 |\tau_1 - \tau_2|^{2H} \cos(\omega_2 \mathcal{T} \tau_2) \\ & \simeq \begin{cases} \frac{2H}{\omega_1 \omega_2 \mathcal{T}^3} \left(\frac{\sin(\omega_1 \mathcal{T})}{\omega_2} + \frac{\sin(\omega_2 \mathcal{T})}{\omega_1} \right), & \text{for } H \in (1/2, 1), \\ \frac{\cos(\pi H) \Gamma(2H+1) (\omega_2^{2H} - \omega_1^{2H})}{\omega_1^{2H} \omega_2^{2H} (\omega_2^2 - \omega_1^2) \mathcal{T}^{2H+2}}, & \text{for } H \in (0, 1/2), \end{cases} \end{aligned} \quad (\text{A.16})$$

where we took advantage of the identity

$$\int_0^\infty u^{2H+1} du \cos(\lambda u) E_{2,2(H+1)}(-u^2) = \frac{\cos(\pi H)}{|\lambda|^{2H} (1 - \lambda^2)}, \quad (\text{A.17})$$

which holds for $H \in (0, 1/2)$. Comparing equations (A.12) and (A.9), we infer that the dominant contribution to the large- \mathcal{T} behaviour of $W_{cc}(\omega_1, \omega_2; \mathcal{T})$ is provided by the latter, such that W_{cc} has the following asymptotic form

$$W_{cc}(\omega_1, \omega_2; \mathcal{T}) \simeq \frac{2D \sin(\omega_1 \mathcal{T}) \sin(\omega_2 \mathcal{T})}{\omega_1 \omega_2} \mathcal{T}^{2H-1}, \quad (\text{A.18})$$

which is valid for any H .

Further on, inspecting the kernels in the integrals in equations (A.12)–(A.14), we realise that the large- u tails do not decay fast enough to ensure the convergence of the integrals even in the sub-diffusive case. Performing some rather straightforward calculations, we then find that for any $H \in (0, 1)$ the leading asymptotic behaviour of the integrals is given by

$$\begin{aligned} & \int_0^1 d\tau_1 \cos(\omega_1 \mathcal{T} \tau_1) \int_0^1 d\tau_2 |\tau_1 - \tau_2|^{2H} \sin(\omega_2 \mathcal{T} \tau_2) \simeq \frac{\sin(\omega_1 \mathcal{T})}{\omega_1 \omega_2 \mathcal{T}^2}, \\ & \int_0^1 d\tau_1 \sin(\omega_1 \mathcal{T} \tau_1) \int_0^1 d\tau_2 |\tau_1 - \tau_2|^{2H} \cos(\omega_2 \mathcal{T} \tau_2) \simeq \frac{\sin(\omega_2 \mathcal{T})}{\omega_1 \omega_2 \mathcal{T}^2}, \end{aligned} \quad (\text{A.19})$$

and

$$\int_0^1 d\tau_1 \sin(\omega_1 \mathcal{T} \tau_1) \int_0^1 d\tau_2 |\tau_1 - \tau_2|^{2H} \sin(\omega_2 \mathcal{T} \tau_2) \simeq -\frac{\cos(\omega_1 \mathcal{T}) + \cos(\omega_2 \mathcal{T})}{\omega_1 \omega_2 \mathcal{T}^2}. \quad (\text{A.20})$$

Taking into account the expressions (A.9), we eventually find

$$\begin{aligned} W_{cs}(\omega_1, \omega_2; \mathcal{T}) & \simeq -\frac{2D \sin(\omega_1 \mathcal{T}) \cos(\omega_2 \mathcal{T})}{\omega_1 \omega_2} \mathcal{T}^{2H-1}, \\ W_{cs}(\omega_1, \omega_2; \mathcal{T}) & \simeq -\frac{2D \cos(\omega_1 \mathcal{T}) \sin(\omega_2 \mathcal{T})}{\omega_1 \omega_2} \mathcal{T}^{2H-1}, \end{aligned} \quad (\text{A.21})$$

and

$$W_{ss}(\omega_1, \omega_2; \mathcal{T}) \simeq \frac{2D \cos(\omega_1 \mathcal{T}) \cos(\omega_2 \mathcal{T})}{\omega_1 \omega_2} \mathcal{T}^{2H-1}, \quad (\text{A.22})$$

which yields our asymptotic expression for $J_{\text{FBM}}(\omega_1, \omega_2)$, equation (50).

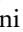
ORCID iDs

Alessio Squarcini  <https://orcid.org/0000-0001-9447-6621>

Enzo Marinari  <https://orcid.org/0000-0002-3464-4133>

Gleb Oshanin  <https://orcid.org/0000-0001-8467-3226>

Luca Peliti  <https://orcid.org/0000-0002-1371-100X>

Lamberto Rondoni  <https://orcid.org/0000-0002-4223-6279>

References

- [1] Priestley M B 1981 *Spectral Analysis and Time Series* vol 1 (New York: Academic)
- [2] Flandrin P 1989 On the spectrum of fractional Brownian motions *IEEE Trans. Inf. Theory* **35** 197
- [3] Niemann N, Kantz H and Barkai E 2013 Fluctuations of $1/f$ noise and the low-frequency cutoff paradox *Phys. Rev. Lett.* **110** 140603
- [4] Leibovich N and Barkai E 2015 Aging Wiener–Khinchin theorem *Phys. Rev. Lett.* **115** 080602
- [5] Leibovich N, Dechant A, Lutz E and Barkai E 2016 Aging Wiener–Khinchin theorem and critical exponents of $1/f^\beta$ noise *Phys. Rev. E* **94** 052130
- [6] Bénichou O, Krapivsky P L, Mejía-Monasterio C and Oshanin G 2016 Temporal correlations of the running maximum of a Brownian trajectory *Phys. Rev. Lett.* **117** 080601
- [7] Dean D S, Iorio A, Marinari E and Oshanin G 2016 Sample-to-sample fluctuations of power spectrum of a random motion in a periodic Sinai model *Phys. Rev. E* **94** 032131
- [8] Berg-Sørensen K and Flyvbjerg H 2004 Power spectrum analysis for optical tweezers *Rev. Sci. Instrum.* **75** 594
- [9] Majumdar S N and Oshanin G 2018 Spectral content of fractional Brownian motion with stochastic reset *J. Phys. A: Math. Theor.* **51** 435001
- [10] Squarcini A, Marinari E and Oshanin G 2020 Passive advection of fractional Brownian motion by random layered flows *New J. Phys.* **22** 053052
- [11] Mejía-Monasterio C, Nechaev S, Oshanin G and Vasilyev O 2020 Tracer diffusion on a crowded random Manhattan lattice *New J. Phys.* **22** 033024
- [12] Voss R and Clarke J 1975 $1/f$ -noise in music and speech *Nature* **258** 31
- [13] Hennig H, Fleischmann R, Fredebohm A, Hagmayer Y, Nagler J, Witt A, Theis F J and Geisel T 2011 The nature and perception of fluctuations in human musical rhythms *PLoS One* **6** e26457
- [14] Balandin A A 2013 Low-frequency $1/f$ noise in graphene devices *Nat. Nanotechnol.* **8** 54
- [15] Weber R O and Talkner P 2001 Spectra and correlations of climate data from days to decades *J. Geophys. Res.* **106** 20131
- [16] Frantsuzov P A, Volkán-Kacsó S and Jankó B 2013 Universality of the fluorescence intermittency in nanoscale systems: experiment and theory *Nano Lett.* **13** 402
- [17] Sornette A and Sornette D 1989 Self-organized criticality and earthquakes *Europhys. Lett.* **9** 197
- [18] Krapf D 2013 Nonergodicity in nanoscale electrodes *Phys. Chem. Chem. Phys.* **15** 459
- [19] Zorkot M, Golestanian R and Bonthuis D J 2016 The power spectrum of ionic nanopore currents: the role of ion correlations *Nano Lett.* **16** 2205
- [20] Sadegh S, Barkai E and Krapf D 2014 $1/f$ noise for intermittent quantum dots exhibits non-stationarity and critical exponents *New J. Phys.* **16** 113054
- [21] Weiss M 2013 Single-particle tracking data reveal anticorrelated fractional Brownian motion in crowded fluids *Phys. Rev. E* **88** 010101
- [22] Li L, Cox E C and Flyvbjerg H 2011 Dicty dynamics: dictyostelium motility as persistent random motion *Phys. Biol.* **8** 046006
- [23] Pedersen J N, Li L, Grádinaru C, Austin R H, Cox E C and Flyvbjerg H 2016 How to connect time-lapse recorded trajectories of motile microorganisms with dynamical models in continuous time *Phys. Rev. E* **94** 062401
- [24] Ciliberto S, Imparato A, Naert A and Tanase M 2013 Heat flux and entropy produced by thermal fluctuations *Phys. Rev. Lett.* **110** 180601
- [25] Ciliberto S, Imparato A, Naert A and Tanase M 2013 Statistical properties of the energy exchanged between two heat baths coupled by thermal fluctuations *J. Stat. Mech.* P12014
- [26] Squarcini A, Solon A and Oshanin G 2022 Spectral density of individual trajectories of an active Brownian particle *New J. Phys.* **24** 013018
- [27] Squarcini A, Gironella M, Sposini V, Grebenkov D S, Metzler R, Ritort F and Oshanin G Anomalous diffusion engaged by an optical tweezer: power spectral density of trajectories (in preparation)
- [28] Fox Z R, Barkai E and Krapf D 2021 Aging power spectrum of membrane protein transport and other subordinated random walks *Nat. Commun.* **12** 6162
- [29] Riechers P M and Crutchfield J P 2021 Fraudulent white noise: flat power spectra belie arbitrarily complex processes *Phys. Rev. Res.* **3** 013170
- [30] Krapf D, Marinari E, Metzler R, Oshanin G, Xu X and Squarcini A 2018 Power spectral density of a single Brownian trajectory: what one can and cannot learn from it *New J. Phys.* **20** 023029
- [31] Krapf D et al 2019 Spectral content of a single non-Brownian trajectory *Phys. Rev. X* **9** 011019
- [32] Sposini V et al Towards a robust criterion of anomalous diffusion *Commun. Phys.* (submitted)
- [33] Sposini V, Metzler R and Oshanin G 2019 Single-trajectory spectral analysis of scaled Brownian motion *New J. Phys.* **21** 073043
- [34] Sposini V, Grebenkov D S, Metzler R, Oshanin G and Seno F 2020 Universal spectral features of different classes of random-diffusivity processes *New J. Phys.* **22** 063056
- [35] Cerasoli S, Ciliberto S, Marinari E, Oshanin G, Peliti L and Rondoni L 2022 Spectral fingerprints of non-equilibrium dynamics: the case of a Brownian gyrotor *Phys. Rev. E* **106** 014137
- [36] Squarcini A, Marinari E, Oshanin G, Peliti L and Rondoni L 2022 Noise-to-signal ratio of single-trajectory spectral densities in centered Gaussian processes *J. Phys. A: Math. Theor.* **55** 405001
- [37] Wick G C 1950 The evaluation of the collision matrix *Phys. Rev.* **80** 268
- [38] Exartier R and Peliti L 1999 A simple system with two temperatures *Phys. Lett. A* **261** 94
- [39] Filliger R and Reimann P 2007 Brownian gyrotor: a minimal heat engine on the nanoscale *Phys. Rev. Lett.* **99** 230602
- [40] Argun A, Soni J, Dabelow L, Bo S, Pesce G, Eichhorn R and Volpe G 2017 Experimental realization of a minimal microscopic heat engine *Phys. Rev. E* **96** 052106
- [41] Crisanti A, Puglisi A and Villamaina D 2012 Nonequilibrium and information: the role of cross correlations *Phys. Rev. E* **85** 061127
- [42] Dotsenko V, Maciolek A, Vasilyev O and Oshanin G 2013 Two-temperature Langevin dynamics in a parabolic potential *Phys. Rev. E* **87** 062130
- [43] Grosberg A Y and Joanny J-F 2015 Nonequilibrium statistical mechanics of mixtures of particles in contact with different thermostats *Phys. Rev. E* **92** 032118

- [44] Mancois V, Marcos B, Viot P and Wilkowski D 2018 Two-temperature Brownian dynamics of a particle in a confining potential *Phys. Rev. E* **97** 052121
- [45] Lahiri S, Nghe P, Tans S J, Rosinberg M L and Lacoste D 2017 Information-theoretic analysis of the directional influence between cellular processes *PLoS One* **12** e0187431
- [46] Cerasoli S, Dotsenko V, Oshanin G and Rondoni L 2018 Asymmetry relations and effective temperatures for biased Brownian gyrators *Phys. Rev. E* **98** 042149
- [47] Cerasoli S, Dotsenko V, Oshanin G and Rondoni L 2021 Time-dependence of the effective temperatures of a two-dimensional Brownian gyrator with cold and hot components *J. Phys. A: Math. Theor.* **54** 105002
- [48] Tyagi N and Cherayil B J 2020 Thermodynamic asymmetries in dual-temperature Brownian dynamics *J. Stat. Mech.* **113204**
- [49] Lucente D, Baldassarri A, Puglisi A, Vulpiani A and Viale M 2022 Inference in non-equilibrium systems from incomplete information: the case of linear systems and its pitfalls (arXiv:2205.08961)
- [50] Ciliberto S 2020 Autonomous out-of-equilibrium Maxwell's demon for controlling the energy fluxes produced by thermal fluctuations *Phys. Rev. E* **102** 050103
- [51] Alberici D, Macris N and Mingione E 2021 Stationary non-equilibrium measure for a dynamics with two temperatures and two widely different time scales (arXiv:2112.11356v1)
- [52] Battle C, Broedersz C P, Fakhri N, Geyer V F, Howard J, Schmidt C F and MacKintosh F C 2016 Broken detailed balance at mesoscopic scales in active biological systems *Science* **352** 604
- [53] Li J, Horowitz J M, Gingrich T R and Fakhri N 2019 Quantifying dissipation using fluctuating currents *Nat. Commun.* **10** 1666
- [54] Sou I, Hosaka Y, Yasuda K and Komura S 2019 Non-equilibrium probability flux of a thermally driven micromachine *Phys. Rev. E* **100** 022607
- [55] Dotsenko V, Maciolek A, Oshanin G, Vasilyev O and Dietrich S 2019 Current-mediated synchronization of a pair of beating non-identical flagella *New J. Phys.* **21** 033036
- [56] Mandelbrot B B and Van Ness J W 1968 Fractional Brownian motions, fractional noises and applications *SIAM Rev.* **10** 422
- [57] Dzhaparidze K and van Zanten H 2004 A series expansion of fractional Brownian motion *Probab. Theory Relat. Fields* **130** 3955
- [58] Gorenflo R, Kilbas A A, Mainardi F and Rogosin S V 2014 *Mittag-Leffler Functions, Related Topics and Applications* (Berlin: Springer)